FLOWFIELD AND ACOUSTIC MEASUREMENTS OF LOW REYNOLDS NUMBER JETS IN THE TRANSONIC RANGE

By

JAMES LYNN STROMBERG

Bachelor of Science in Mechanical Engineering

Oklahoma State University

Stillwater, Oklahoma

1976

Submitted to the Faculty of the Graduate College
of the Oklahoma State University
in partial fulfillment of the requirements
for the Degree of
MASTER OF SCIENCE
July, 1978

Thesis
1978
S921f
Cop. 2

OKLAHOMA STATE UNIVERSITY LIBRARY

FLOWFIELD AND ACOUSTIC MEASUREMENTS OF LOW REYNOLDS NUMBER JETS IN THE TRANSONIC RANGE

Thesis Approved:

Dennis K McLaughlin
Thesis Adviser

W. A. Liederman

Ladislaus J. Fila

Norman N. Durham
Dean of the Graduate College

1012034

ACKNOWLEDGEMENTS

The author would like to recognize the National Science Foundation (Grant No. ENG 75-21405) and the National Aeronautics and Space Administration (Grant No. NSG 1467) whose financial support made this study possible.

The author also wishes to express his deepest appreciation to his major adviser, Professor Dennis K. McLaughlin, and to his other committee members, Professor W. G. Tiederman, and Professor L. J. Fila, for their advice and guidance concerning this work. Appreciation is also expressed to Dr. G. L. Morrison, Dr. T. R. Troutt, and Mr. J. D. Swearingen, fellow graduate students working on this project, and to Velda Davis and Debbie Reimer whose expert typing and knowledge of the Graduate College's rules were invaluable.

TABLE OF CONTENTS

LIST OF TABLES

LIST OF FIGURES

NOMENCLATURE

a_o	speed of sound in the ambient air
a_w	hot-wire resistance overheat, $\frac{R_w - R_{aw}}{R_{aw}}$
ALS	arbitrary linear scale
A_ρ	density fluctuation sensitivity coefficient
A_u	velocity fluctuation sensitivity coefficient
A_T	stagnation temperature fluctuation sensitivity coefficient
c	axial wave speed
d	diameter of the hot-wire
D	nozzle exit diameter
e'	fluctuating hot-wire voltage
$\overline{E}$	mean hot-wire voltage
f	frequency (Hz)
k	complex wave number
k_i	imaginary part of the complex wave number
k_r	real part of the complex wave number
ℓ	length of the hot-wire
M	Mach number
n	azimuthal mode number
P	pressure
P_{atm}	standard atmospheric pressure
P_c	test chamber pressure
P_o	local jet stagnation pressure

P_t	upstream total pressure
r	radial distance from jet centerline
Re	Reynolds number
R_{aw}	adiabatic hot-wire resistance
R_w	hot-wire resistance
St	Strouhal number, fd/U
T	static temperature
T_o	stagnation temperature
T_o'	stagnation temperature fluctuations
T_w	hot-wire temperature
u	axial velocity
U	mean centerline jet velocity at the exit
$\overline{V}$	mean velocity in the axial direction
x	downstream distance from the nozzle exit
x_c	length of the potential core
y	vertical distance from the centerline
z	horizontal distance from the centerline
θ	azimuthal angle
λ	axial wavelength
ρ	density
ρ_o	density of ambient air
ρ_t	stilling chamber total density
φ	relative phase
ω	frequency (radians/sec.)
$(\overline{\ })$	mean quantity
$(\ )_{rms}$	root mean square of a fluctuating quantity
$\langle\ \rangle$	phase average

CHAPTER I

INTRODUCTION

Background

The first theoretical formulation for the production of aerodymanic noise in high speed jets was developed by Lighthill (1, 2). This first theory was formulated for the subsonic flow regime by rewriting the governing equations for arbitrary fluid motion. By separating the linear and nonlinear terms, Lighthill obtained an equation for acoustic wave propagation caused by fluctuating flow quantities. Using the same approach, Ffowcs Williams (3) extended this work into the supersonic flow regime.

For many years the source terms--those due to fluctuating flow--of Lighthill's equation were assumed to be of a completely random nature, i.e., turbulence with a random distribution of length and time scales. Experimental measurements of turbulent flows supported this assumption with results such as spectral analyses which revealed very broad frequency content characteristic of random processes.

However, in recent years several researchers including Mollo-Christensen (4), Crow and Champagne (5), Tam (6), and others have focused their attention on large-scale coherent fluctuations as a potential noise source in turbulent flows previously thought to be completely random in nature. These observed large-scale coherent fluctuations are subject to different interpretations. Laufer et al. (7), Lau et al. (8),

Winant and Browand (9), and Dutt (10) interpret these large-scale structures as vortex structures. These interpretations apply to incompressible, subsonic, and supersonic flow regimes. With a different interpretation, Tam (6), Chan (11), Moore (12), and others view these large-scale structures as waves, or wave-like eddies similar to those involved in the transition from laminar to turbulent flow. These views also apply to both subsonic and supersonic flow regimes.

Using a shadowgraph technique in a free shear layer, Brown and Roshko (13) have observed that a large-scale wave-like undulation which first appears at low Reynolds numbers, persists at higher Reynolds numbers, and remains a dominant flow feature at Reynolds numbers where the flow is commonly assumed to be fully turbulent. This observation suggests that considerable understanding can be gained of large-scale structures in fully turbulent flow by observing low Reynolds number transitional flows.

This low Reynolds number approach has been used at Oklahoma State University for supersonic jets and has the distinct advantage of hot-wire utilization not possible in high Reynolds number experimental studies. As a result of this study, McLaughlin, Morrison, and Troutt (14, 15) and Morrison and McLaughlin (16) have determined that the large-scale coherent fluctuations measured in low Reynolds number supersonic jets may be described by a wave-instability model and are dominant noise production mechanisms.

Objectives

In view of this background pertaining to the noise production mechanisms in high speed jets, this research was intended to develop an

understanding of these mechanisms in low Reynolds number transonic jets. The incentive for this study was the previous research at Oklahoma State University on the noise radiation process in supersonic jets. The intended approach was to apply the techniques established in this previous supersonic research, which had its major emphasis on determining the role of large-scale instabilities in the noise production process. In extending these techniques to the transonic range, the major objectives of this study were:

1. to characterize the nature of large-scale flow fluctuations by making hot-wire measurements to determine the growth rate, wavelength, and wavefront orientation of the dominant spectral components;
2. to determine the general properties of the acoustic field with single microphone surveys and two-microphone cross correlations; and
3. to relate the radiated noise to the flow fluctuations to identify and gain understanding of the dominant noise generating mechanisms.

Satisfying the first objective above would demonstrate the validity of describing the large-scale flow fluctuations with a wave-instability model. The model hypothesized consists of the linearized instability equations for parallel transitional flow. The equations for this model have solutions for any fluctuation flow quantity in the form

$$q\,(r, x, \theta, t) = \hat{q}\,(r)\ \mathrm{Real}[\exp i(kx - \omega t - n\theta)]$$

where k is the complex wave number, ω is the angular frequency of the disturbance, and n is the azimuthal mode number.

All jets studied were low Reynolds number, Mach numbers 0.90, 1.0, and 1.1. A thorough investigation was conducted on the Mach number 0.90 jet and representative measurements were made of the Mach numbers 1.0 and 1.1 jets to establish Mach number dependence in the transonic range.

CHAPTER II

EXPERIMENTAL APPARATUS

Facility

All measurements for this research were made in the Oklahoma State University jet noise facility. The test chamber is shown schematically in Figure 1. The jet exhausts into this 114 cm. x 76 cm. x 71 cm. vacuum test chamber which is lined with five centimeter Scott Pyrell acoustic foam. This produces an anechoic environment for frequencies above one kilohertz. The reverberant pressure field has been estimated to be less than two db for the range of frequencies encountered during these measurements. The static pressure within the chamber is controlled by evacuating the air through a variable throat diffuser with a 0.1 m^3/sec. Kinney vacuum pump. Vacuum pump pressure fluctuations were effectively dampened by isolating the pump from the test chamber with a 30 cubic meter storage tank.

Upstream of the nozzle are a contraction section (area ratio 325:1), stilling section, throttling valve, pressure regulator, high pressure storage tank, air dryer, and air compressor. These are shown in Figure 2 which is a schematic of the entire facility. The 1.8 cubic meter storage tank is of sufficient volume to allow the air compressor (and accompanying pressure fluctuations) to be shut down during experimental operation. The cylindrical stilling section is 55 cm. long with a 14.3 cm. inside diameter. It consists of five centimeters of foam,

three perforated plates, a 7.6 cm. honeycomb section, and six fine mesh screens. The contraction section (with a cubic contour) matches the stilling section to the nozzle as shown schematically in Figure 3. The nozzle used for all measurements had a converging contour followed by a short parallel flow section. The contour coordinates were obtained from Smith and Wang (17) who designed the contour for parallel flow using inviscid theory.

The facility test chamber is equipped with a probe drive capable of translation in three orthogonal directions. Various probe adapters may be attached to the basic probe drive system to facilitate the use of hot-wire probes, Pitot or static pressure probes, or microphones. In addition to the probe drive system, a second stationary probe mount is attached to the top of the test chamber. Prior to an experiment, this stationary probe mount can be adjusted in two orthogonal directions in the vertical plane of the jet centerline. The coordinate system used for the probe drive as well as all experimental results is shown in Figure 4.

Precision ten-turn potentiometers provide the probe drive system with DC voltages proportional to the probe location. This system allows accurate and repeatable probe positioning when care is taken to eliminate mechanical backlash.

The facility is equipped with an artificial exciter similar to that used by Kendall (18) and reported earlier by McLaughlin et al. (14). The exciter consists of a 1/16 inch tungsten electrode insulated with ceramic tubing. The electrode--mounted at the nozzle exit--produces an oscillating glow discharge (ionization of the air) when subjected to an alternating voltage biased to a large negative potential (400 V DC).

The glow discharge effectively puts a small controlled disturbance in the jet. When excited at the jet's natural instability frequencies, the jet's flow and acoustic properties will phase-lock to this small disturbance.

Instrumentation

Pressure measurements were made with a silicone oil (specific gravity of 0.93) manometer referenced to an absolute pressure of 50 microns of mercury. Both Pitot and static pressure probes were used. The Pitot probe consists of a 0.53 mm (outside diameter) square-ended tube attached to a thin brass wedge. The static pressure probe (0.53 mm outside diameter) is of similar construction with its upstream end fitted with a slender cone. Both pressure probes are shown schematically in Figure 5.

The hot-wire probes were constructed by attaching Disa 55A53 subminiature hot-wires to a slender wedge similar to that of the Pitot probe. Both horizontal and vertical hot-wires were constructed in this manner for use in the bottom and side shear layers, respectively. A frequency response of 40 kHz or more was obtained using a Disa 55M01 constant temperature anemometer (main frame) with a Disa 55M10 standard bridge.

The jet's acoustic field was measured with Bruel and Kjaer 1/8 inch diameter type 4138 condenser microphones, model 2618 preamplifiers, and a two-channel model 2804 power supply. The output of this equipment is effectively omni-directional, since the response is within ± 3 db for frequencies up to 60 kHz. The microphones were calibrated using a Bruel and Kjaer type 4220 piston phone. In previous experiments it has

been observed by McLaughlin et al. (15) that the microphone calibration is not affected by the low pressure environments.

A Tektronics 7L5 spectrum analyzer was used to obtain both hot-wire and microphone spectra. All spectra were recorded by photographing the analyzer's display CRT. A Saicor model SAI 43A correlation and probability analyzer was used for all phase-averaging and correlations of hot-wire, microphone, and exciter signals.

CHAPTER III

PROCEDURE

Calculation of Mach Number

Desired nozzle exit Mach numbers and Reynolds numbers were set by independent control of the upstream total pressure P_t and the test chamber pressure P_c. The upstream total pressure was controlled by reducing the upstream reservoir pressure with a regulator valve and then throttling this reduced pressure with a needle valve just upstream of the stilling section. The test chamber pressure was controlled with a variable throat diffuser mounted at the test chamber exit (see Figure 2).

Pitot pressure measurements of the local stagnation pressure at the jet exit, P_o, showed that there were no significant losses in total pressure through the nozzle. Static pressure probe measurements showed that the test chamber pressure, P_c, is a good measure of the static pressure, P, throughout the jet. With these assumptions ($P = P_c$ and $P_o = P_t$) P/P_t was determined from the measured P_c and P_t; and hence the Mach number was calculated from the isentropic relation for P/P_t.

Hot-Wire Procedure

All hot-wire measurements were made with the hot-wire perpendicular to the flow. With the exception of azimuthal phase measurements, the hot-wire was also tangent to the shear annulus and in most cases at a

radial location of maximum hot-wire fluctuating voltage e'_{rms}. To minimize probe interference, hot-wire measurements were generally made in the bottom shear layer.

The frequency response of the various hot-wires varied from 40 to 70 kHz. This was well above the frequencies of the fluctuations measured in the flowfield. The output from the hot-wire was high pass filtered at 1.5 kHz and low pass filtered at 60 kHz. These settings were chosen to be consistent with those of the microphone.

Microphone Procedure

The test chamber has a resonance of approximately 500 Hz. All microphone signals were high pass filtered at 1.5 kHz to eliminate the portion of the signal due to this resonance. The microphone signal was also low pass filtered at 60 kHz. This eliminated the portion of the signal due to the microphone resonance at 100 kHz which occurs in low pressure environments.

Sound pressure level measurements and microphone spectra were made with the microphone in the vertical plane of the jet centerline assuming the acoustic field was axisymmetric. When making microphone cross correlations to determine the azimuthal phase dependence of the excited jet, a fixed microphone was positioned above the jet while a movable microphone was traversed 180 degrees in the azimuthal direction. Both the fixed and movable microphones remained at the same radial location in the acoustic field as shown schematically in Figure 6. Data for points between 180 and 360 degrees were obtained by rotating the nozzle and consequently the exciter, which fixed the azimuthal orientation of phase.

The Artificial Exciter

The role of the exciter was essentially to phase-lock the natural instability in the jet and the resulting acoustic radiation. When this was accomplished, relative phase measurements could be made of the hot-wire or microphone signals. For instance the wavelengths of spectral components of the jet's instability were determined by measuring the relative phase between the hot-wire signal and the excitation signal. This was accomplished by cross correlating the hot-wire and exciter signals. Correlations were made at several axial (x/D) positions, and the correlation phase was plotted as a function of x/D. The resulting slope determined the spectral component's wavelength.

Phase-averaged signals were obtained for both hot-wire and microphone signals utilizing the Saicor analyzer in the enhance mode. In this mode the exciter input signal was used to generate the necessary trigger input to the analyzer.

Determination of the Appropriate Experimental Reynolds Number

Since the flowfield characteristics of interest in this study were instabilities, the Reynolds number of the jets to be studied was chosen accordingly. The desired jet behavior was one of laminar flow at the nozzle exit followed by transition to turbulence a few diameters downstream. For very low Reynolds numbers, the hot-wire signal appeared to be affected by edgetones. This was apparent as the frequency of the dominant instability would change as the hot-wire was traversed in the axial direction. This was similar to the edgetone phenomena reported by Wolley and Karamcheti (19). This behavior was observed at a Reynolds

number of 2400. Another problem at this low Reynolds number was insufficient amplitude of the microphone output. Both of these problems were eliminated by increasing the Reynolds number to 3600. However, careful alignment of the hot-wire probe support was necessary since a slight yawed condition would again cause the edgetone phenomena mentioned above. This Reynolds number (3600) was otherwise found to be quite satisfactory for the purposes of this study, and all measurements presented are of jets at this Reynolds number.

CHAPTER IV

RESULTS OF FLOWFIELD MEASUREMENTS

Mean Flow, Mach Number 0.90 Jet

Mean flow profiles were obtained at axial (x/D) locations of 1, 5, and 10 by making Pitot pressure measurements. In determining these profiles it was again assumed that the measured chamber pressure, P_c, is the same as the static pressure in the jet. Probe interference encountered when attempting Pitot measurements above the jet's centerline with a bottom mounted probe made these measurements unreliable, so the measurements were made in only the bottom half of the jet. Figure 7 shows the radial variation in Mach number at three downstream locations.

Centerline Pitot measurements were also made, and Figure 8 shows the axial variation in centerline Mach number. Figure 8 indicates that the shear layers have grown together between 5 and 7 diameters downstream of the nozzle exit. This observation is consistent with Figure 7 since at x/D = 5 the profile shows two distinct shear layers, while at x/D = 10 the shear layers have grown together.

Hot-Wire Spectra and the Coherent Portion of the Hot-Wire Signal, Mach Number 0.90, 1.0, and 1.1 Jets

Hot-wire spectra were obtained at several downstream positions for Mach number 0.90, 1.0, and 1.1 jets. These spectra were taken at the radial position of maximum hot-wire voltage fluctuation (e'_{rms}). In the potential core region this maximum was found in the shear layer while beyond the end of the potential core the maximum fluctuations were found near the centerline.

Figure 9 shows the hot-wire spectra for the Mach number 0.90 natural (unexcited) jet at successive downstream positions. These spectra contain a narrow band of frequency components around a Strouhal (St) number of 0.44 for the first seven diameters downstream of the nozzle exit. At each successive downstream position, the spectra broaden around this dominant spectral component until at x/D = 8 the spectrum is rather broad with the majority of the fluctuations between St = 0.04 and St = 0.82.

It should be noted, for this Mach number 0.90 jet, that if the hot-wire was moved inward from the point of maximum fluctuations toward the inside edge of the shear annulus that an additional spectral component at St = 0.22 appears in the hot-wire spectra. This is shown in Figure 10 which was recorded with the probe in the bottom shear layer at x/D = 4. The presence of this St = 0.22 spectral component in the flowfield is quite important since--as will be seen later--this frequency dominates the acoustic field.

The hot-wire signal was phase-averaged at each downstream location so that the coherent portion of the signal could be separated from the

full wave. The RMS fluctuations of the phase-averaged signal were then compared with the RMS fluctuations of the full wave. In this manner the fraction of the signal that was coherent was determined at each downstream location. Figure 11 shows the axial variation in the coherent fraction of the hot-wire signal. This verifies the apparent spectral broadening and increased randomness at successive downstream positions. This same phenomena was observed by Morrison (20) in supersonic jets.

Figure 12 shows the hot-wire spectra for the Mach number 1.0 natural (unexcited) jet at successive downstream locations. These spectra are less discrete than the Mach number 0.90 jet, but they do have a dominant spectral component. However, the dominant component has shifted from St = 0.44 to St = 0.38. Like the Mach number 0.90 jet, there is an apparent spectral broadening and increased randomness at each successive downstream location. This was again verified by phase-averaging the hot-wire signal and the result is shown in Figure 13 where the axial variation in the coherent fraction of the hot-wire signal is plotted. The Mach number 1.0 jet's spectrum is also quite broad at x/D = 8 and the dominant component at St = 0.38 has disappeared with the lower frequencies becoming more predominant around St = 0.08.

Figure 14 shows the hot-wire spectra for the Mach number 1.1 natural jet at successive downstream locations. At x/D = 2 the spectrum has a single discrete frequency component at St = 0.50. This component at St = 0.50 is still present at x/D = 4 along with some other components of smaller amplitude, one of which is at St = 0.56. This component at St = 0.56 increases in amplitude as x/D is increased and at x/D = 5 its amplitude is greater than that of the St = 0.50 component. At x/D = 6 the St = 0.56 component is the only discrete component remaining in the

the spectrum with the majority of the fluctuations having a frequency between St = 0.05 and St = 0.35. One must be careful with the interpretation of these spectra since the Mach number 1.1 jet was attained by overexpanding a converging nozzle to a supersonic Mach number. Strong cell structures are known to exist in this situation which quite likely influence the frequency content of the fluctuations.

Effect of Excitation on the Flowfield

When the Mach number 0.90 jet is excited at its dominant spectral component (St = 0.44), the resulting hot-wire spectra are effectively unaltered from the natural spectra. The only perceivable change is a slight increase in amplitude of the dominant spectral component (the jet's natural frequency). If the excitation frequency is shifted slightly from the jet's natural frequency, the jet will follow the excitation frequency. This is shown in Figure 15 which is a hot-wire spectrum of the jet excited at St = 0.38. Comparison with Figure 16--which is the natural spectrum at the same location and the same linear scale--shows both the increase in amplitude and frequency shift due to the exciter.

If the exciter frequency was moved still further away from the jet's natural frequency--until it differed by St $\simeq$ 0.13--the jet's natural frequency would reappear and again dominate the flow with a small component still present at the excitation frequency. An example of this is shown in Figure 17 where the hot-wire spectrum was taken with the jet excited at St = 0.60. The spectrum in Figure 17 was also at the same location and linear scale as those in Figures 15 and 16. It should be noted here that the amplitude of the excited component in

Figure 17 is considerably less than the excited component in Figure 15 where the excitation frequency differs only slightly from that of the natural frequency.

The effect of excitation was measured over a broad range of frequencies and plotted in Figure 18. This figure shows both the amplitude of the excited spectral component and the RMS amplitude of the full spectrum plotted as a function of excitation frequency. From this plot it is seen that both the RMS amplitude of the full wave and the amplitude of the excited spectral component have relative maxima around the jet's natural instability frequency (St = 0.44) and its first subharmonic (St = 0.22). This behavior is similar to that seen by Morrison and McLaughlin (16) in supersonic jets. One major difference between these results is the subsonic jet's lack of spectral peaks within a band of unstable frequencies. Another difference is the subsonic jet's increased response around the first subharmonic (St = 0.22) of the jet's natural instability frequency (St = 0.44).

Relative Phase Measurements, Mach Number 0.90

The wavelength and wave orientation of dominant spectral components of the instability were determined by measuring the relative phase of the hot-wire signal referenced to the excitation input signal. In this manner the axial wave number k_r and the azimuthal mode number n are determined.

Figure 19 is a plot of relative phase as a function of axial position for the Mach number 0.90 jet excited at St = 0.22, 0.44, 0.55, and 0.69. A straight line was fit to each set of data using a linear regression.

curve fit. The wavelength was determined from the slope of each line, and the phase velocity calculated from the frequency and the wavelength.

The radial distribution of phase was measured for the St = 0.44 component at x/D = 3 and 5. At both of these locations there is a substantial phase shift of approximately 180 degrees between the top and bottom shear layers. Very rapid phase change occurs in the vicinity of the jet centerline followed by less rapid change across the top and bottom shear layers. This radial phase behavior in the shear layers is similar to that observed by Morrison and McLaughlin (16).

Azimuthal phase measurements were made at St = 0.22 and St = 0.44 to determine the azimuthal mode numbers of these instability components. Difficulties encountered during these measurements somewhat hindered their accuracy, but the data were nonetheless meaningful. One difficulty was the hot-wire's orientation in the shear layer. For instance, a horizontal hot-wire necessarily remained horizontal throughout a given experiment. This meant that the hot-wire became alternately tangent and perpendicular to the shear annulas as it was traversed in the azimuthal direction. A second difficulty was the radial phase behavior of the jet itself, since radial phase measurements showed significant phase change within the shear layer. This behavior caused the radial positioning of the hot-wire to have a significant influence on the azimuthal phase data.

With these difficulties related to the positioning of the hot-wire the results of a single azimuthal phase experiment were questionable, at least when the results showed substantial phase changes as is the case for the helical ($n = \pm 1$) azimuthal mode. For this reason the experiment was repeated several times for the St = 0.44 instability

component. The data from these repeated experiments are shown in Figure 21. The data from Figure 21 were averaged for each azimuthal angle and Figure 22 shows this average azimuthal phase distribution of the St = 0.44 instability component along with a theoretical phase distribution. This theoretical distribution is the superposition of the n = +1 and n = -1 azimuthal modes of equal amplitude. These data indicate that the St = 0.44 instability component has azimuthal mode numbers +1 and -1 simultaneously. This can be interpreted as a flapping of the jet and is the same behavior as that seen by Morrison (20) in supersonic jets.

Figure 23 shows the azimuthal phase distribution for the St = 0.22 component. These data indicate that this instability component has an azimuthal mode number of zero. Dutt (10) has also measured the n = 0, n = 1, and higher modes in the pressure field of a supersonic jet. In addition to the n = 1 mode, the presence of the n = 0 mode is a quite important result for two reasons: (1) other investigators have not excited this mode with a point exciter and have doubted the ability to do so, and (2) these different azimuthal phase behaviors may be responsible for the substantially different effects the St = 0.22 and 0.44 instability components have on the acoustic field. Important consequences with regard to the noise generating effectiveness of these different azimuthal modes are discussed in more detail in Chapter VI.

Growth Rates, Mach Number 0.90 Jet

In order to determine the growth rates of the fluctuating flow quantities it was necessary to decompose the hot-wire voltage fluctuations into the appropriate flow fluctuations, u', ρ', and T_o'. This

decomposition procedure is quite difficult in transonic flow and very few experimenters have attempted it. Horstman and Rose (21) have developed a procedure for obtaining the fluctuating flow quanitites in transonic flows for sensor Reynolds numbers greater than 20 and high sensor overheat ratios.

The procedure of Horstman and Rose could not, however, be used in the present experiments because the maximum sensor Reynolds number was only 1.7 at the jet centerline with even smaller values in the shear annulus. Analysis of the hot-wire voltage fluctuations for this study was accomplished by direct calibration and the procedure is outlined in Appendix A. This technique showed that under the conditions of the present study the hot-wire was sensitive to density fluctuations only. The results of this technique are shown in Figure 25 which shows the axial variation of $\rho'/\overline{\rho}$. The data for this figure were gathered at constant radial locations of x/D = 0.28 and 0.35 for the Strouhal number 0.22 and 0.44 components, respectively. These locations were chosen to maximize the hot-wire fluctuating voltage e'_{rms} for both frequency components. Figure 24 shows that the axial growth of $\rho'/\overline{\rho}$ is approximately exponential for the first few diameters for both frequency components. The growth rates $-k_i$ were determined for both of these frequency components (St = 0.22 and 0.44) and are included in Table I.

CHAPTER V

RESULTS OF ACOUSTIC MEASUREMENTS

Sound Pressure Level Contours, Mach Number 0.90 Jet

When measuring sound pressure levels in the vacuum chamber, the reference pressure was scaled to the ambient pressure in the chamber. This scaling allowed the sound pressure levels measured in the vacuum chamber to be compared with sound pressure levels measured at atmosheric conditions. This scaling was accomplished by calculating the sound pressure level in the following manner:

$$SPL = 20 \log_{10} \frac{P'_{rms}}{(2 \times 10^{-5} \text{ N/m}^2)(P_c/P_{atm})}$$

Sound pressure level contours of the Mach number 0.90 jet are plotted in Figure 25. This experiment was repeated with a second microphone and the results agreed in all cases within ± 1 db. Figure 26 is a plot of SPL contours of a similar jet (M = 0.90) at a much higher Reynolds number measured by Mollo-Christensen et al. (22). The shape and amplitude of the two jets' contours are very similar when the low Reynolds number contour is displaced about 5 diameters upstream from the high Reynolds number contour. McLaughlin et al. (1977) showed that the displacement of the sound pressure level contours was directly related to the displacement of the region of maximum flow fluctuations

in supersonic jets. The data here demonstrate the same feature. From the shape of the sound pressure level contours it is also apparent that the low Reynolds number jet noise emission is more directional than that of the high Reynolds number case. This directional behavior can be seen in Figure 27 which presents SPL directivity distributions for both the low and high Reynolds number jets discussed above. These data are discussed in more detail in Chapter VI.

Microphone Spectra, Mach Number 0.90, 1.0, and 1.1 Jets

For the Mach number 0.90 jet microphone spectra were obtained at a constant r/D (r/D = 6) and at various values of x/D. These spectra showed that the frequency content of the radiated noise was very similar at all observed axial locations ($4 < x/D < 25$). The spectrum obtained at x/D = 20 in the maximum SPL lobe is shown in Figure 28 along with a far field spectrum for the same jet. These spectra are rather broad banded but have a peak at St = 0.22. A spectrum obtained at a position closer to the jet centerline (r/D = 3.5, x/D = 10) was similarly broad banded and also had a peak. However, this observed peak was at St = 0.44. This spectrum is shown in Figure 29.

For both the Mach number 1.0 and 1.1 jets a microphone spectrum was obtained in the maximum SPL lobe to obtain information concerning the frequency content of its source. Since SPL contours were not available for these jets, the microphone position for these spectra was found by traversing the microphone in the axial direction--at a constant radial distance--to the location of maximum SPL. These spectra are shown in Figure 30. Far field microphone spectra were also obtained for

these jets and are shown in Figure 31. By comparing these near field and far field spectra with the hot-wire spectra for the same jets shown in Figures 12 and 14, it is observed that the frequency content of the acoustic field and the frequency content of the flowfield have common dominant spectral components for the Mach number 1.0 jet. This is not the case with the Mach number 1.1 jet since the acoustic field and flowfield have a dominant band of frequencies around St = 0.33 and 0.56, respectively. This was not expected since the low Reynolds number supersonic jets of previous studies have had the same frequency components dominant in both the flowfields and acoustic fields (14, 16). As mentioned in Chapter IV, this discrepancy is probably due to the effect of the strong cell structure present in the Mach number 1.1 jet.

Effect of Excitation on the Acoustic Field, Mach Number 0.90 Jet

Microphone spectra were observed in the maximum SPL lobe (r/D = 6, x/D = 20) of the Mach number 0.90 jet excited at various frequencies. At this location the natural jet's spectra were broad banded with a peak at St = 0.22. When the jet was excited at St = 0.22, the only noticeable effect on the noise spectra was a slight increase in the peak at St = 0.22. If the excitation frequency was varied from this frequency of the natural peak, the peak of the excited spectra would lose amplitude and follow the frequency of excitation. This behavior was observed over a wide range of excitation frequencies and is plotted in Figure 32. It is important that the acoustic field's response is the highest at an excitation Strouhal number of 0.22 in comparison with

the flow fluctuations which have a maximum response at an excitation frequency of St = 0.44 (as shown in Figure 18).

Azimuthal Phase and Coherent Portion of the Microphone Signal, Mach Number 0.90 Jet

Microphone azimuthal phase measurements were made of the excited Mach number 0.90 jet. The microphone setup is shown in Figure 6. The azimuthal phase data were obtained by cross correlating the signals from the two microphones for various locations of the lower microphone. In this manner the acoustic field's azimuthal phase dependence was determined for the St = 0.22 component. This phase dependence is shown in Figure 33 to be axisymmetric (n = 0).

Also determined during this experiment was the phase-averaged microphone signal at each position of the lower microphone. The RMS fluctuations of the phase-averaged signal was then compared with the RMS fluctuations of the full wave. In this manner it was determined what fraction of the signal was coherent at each azimuthal location. These data along with the sound pressure level of the full spectrum are plotted in Figure 34. From this figure it can be seen that the full spectrum SPL maximizes at an azimuthal location of $\theta = 0^{o}$ (location of the point exciter) and minimizes at $\theta = -90^{o}$ (and probably $+90^{o}$). The opposite is true for the coherent fraction of the microphone signal. With the jet excited at St = 0.22 the frequency of the radiated noise is quite discrete at St = 0.22. Figure 33 has shown this frequency component of the acoustic field to be of axisymmetric mode (n = 0). Therefore, the non-axisymmetric behavior seen in Figure 34 may be due to the flapping ($n = \pm 1$) component of instability at St = 0.44

radiating more noise in the direction of the flapping (0^{o} and 180^{o}). It appears that the noise radiated from this flapping component of instability (at St = 0.44) is not phase-locked with that radiated from the axisymmetric component (at St = 0.22). Thus, the phase-averaged signal ($\langle e' \rangle_{rms}$) which is predominantly of frequency St = 0.22 is not dependent on the azimuthal location of the microphone. Consequently, the coherent fraction of microphone signal $\{\langle e' \rangle_{rms}/e'_{rms}(\text{full spectrum})\}$* was anti-correlated with the full spectrum SPL.

Determination of the azimuthal phase behavior for the St = 0.44 component with microphone cross correlations was not possible. As previously mentioned, the acoustic field would not respond to excitation above St = 0.28; and excitation was necessary since the noise spectra of the natural jet was too broad to allow correlations.

---

*Recall that the sound pressure level (SPL) in Figure 34 is simply the logarithm of e'_{rms} (full spectrum).

CHAPTER VI

DISCUSSION AND CONCLUSIONS

Mach Number 0.90 Jet

The SPL directivity distribution presented in Figure 27 shows that the low Reynolds number (3.7×10^3), Mach number 0.90 jet is from 2 db to 5 db louder than the higher Reynolds number (5.4×10^5) jet of the same Mach number measured by Mollo-Christensen et al. (22). This at first appears unreasonable, since the noise radiated from a low Reynolds number jet was not expected to be any louder than that from a high Reynolds number jet. One source of discrepancy is that the data from this study were not corrected for the reverberant field which was estimated to be less than 2 db. The instrumentation uncertainties for the present study have been estimated to be ± 1 db. One notable physical difference in the jets being compared is that the high Reynolds number jet measured by Mollo-Christensen exited from a nozzle that was equipped with boundary layer suction. It should also be noted that the facility used in these high Reynolds number measurements had been given extraordinary attention to eliminate extraneous sources of sound and turbulence. For example, the microphone was hung from a boom using loosely spun cotton twine.

With these possibilities for discrepancies, it is quite possible that the low Reynolds number jet used in this study produces no more noise than the high Reynolds number jet with which it was compared.

However, in all probability it is just as loud. McLaughlin, Morrison, and Troutt (14, 15) have found this to be true of low Reynolds number supersonic jets. This result suggests that the large-scale coherent fluctuations in the flowfield of the low Reynolds number, Mach number 0.90 jet may be the dominant noise production mechanism.

These large-scale fluctuations in the flowfield--as shown by hot-wire spectra--persist for several diameters downstream of the nozzle exit and appear to be the jet's initial instabilities encountered during transition from laminar to turbulent flow. This observation is supported by the experimenter's ability to measure all the quantities predicted by the solution to the linearized instability equations for parallel flow. These quantities are growth rate $-k_i$, wave number k_r, and azimuthal mode number n. The measurements of these quantities were reported in Chapter IV and are summarized in Table I. Also included in Table I are the same quantities (k_i, k_r, and n) measured by Chan (23) in a subsonic jet and Morrison and McLaughlin (16) in supersonic jets.

The growth rates presented in Table I are the initial growth rates, i.e., those measured in the region just downstream of the nozzle exit where transition from laminar to turbulent flow occurs. The values obtained in this study ($-k_iD = 1.7$ for the St = 0.22 component and $-k_iD = 2.1$ for the St = 0.44 component) were obtained by a least-squares exponential curve fit to the fluctuating flow data in this region of transition (shown in Figure 24). The values thus obtained appear reasonable when compared to the growth rates reported by Chan (23) in a subsonic jet and Morrison and McLaughlin (16) in supersonic jets (see Table I).

The hot-wire spectra show that the jet's unstable frequencies are St = 0.22 and St = 0.44. The St = 0.44 instability component appears to be the most dominant component in the flowfield since in the shear layer at a radial position of maximum hot-wire fluctuating voltage e'_{rms}, this component appears solely. However, if the hot-wire is moved inward toward the jet centerline from the point of maximum e'_{rms}, the St = 0.22 instability component is found and is of similar magnitude to the St = 0.44 component at that position in the shear layer.

As shown in Chapter IV, the St = 0.22 instability component has an azimuthal mode number of zero, while the St = 0.44 component has mode numbers n = +1 and -1 simultaneously. Dahan and Elias (24) have measured both the axisymmetric mode (n = 0) and the helical mode (n = 1) in the acoustic field of a hot subsonic jet. Chan (11) has observed both these modes (n = 0 and n = 1) and the double helical mode (n = 2) in the flowfield pressure fluctions of an incompressible jet. Dutt (10) has also observed these modes (n = 0 and n = 1) and higher modes in the near acoustic field of a turbulent supersonic jet. In a different but related flowfield (the supersonic cone wake) several azimuthal modes (n = 1, 2, 3) were measured by McLaughlin (25).

Some of the experimental findings of these previous studies have shown that the magnitudes of the observed quantities vary substantially for different azimuthal modes. Dahan and Elias (24) found that the power spectral density of the axisymmetric (n = 0) mode was an order of magnitude larger than that of the helical (n = 1) mode in the radiated noise from a hot subsonic jet. Chan (11) found the axisymmetric (n = 0) flowfield pressure fluctuations in the middle of the shear

layer to be as much as 15 db higher than the helical (n = 1) fluctuations in an incompressible jet.

Theories have been formulated which predict that sound emitting efficiencies will vary for flow fluctuations of different azimuthal modes. One of these has been developed by Morris and Tam (26) for supersonic jets; and it predicts that for equal initial amplitudes, the axisymmetric (n = 0) instability radiates approximately 8 db more noise than the helical (n = 1) mode for St < 0.5. Michalke and Fuchs (27) have also developed a theory concerning the noise radiation efficiencies of different azimuthal modes in subsonic jets due to mean flow-turbulence interaction. In their model only five percent of the mean square velocity fluctuations were axisymmetric (n = 0), but 42 percent of the mean square flowfield pressure fluctuations were of this mode (n = 0).

These results, both experimental and theoretical, indicate that the axisymmetric (n = 0) mode is a much more effective noise producer than the helical (n = 1) or higher modes. The findings of this study support these previous results in that the axisymmetric (n = 0) flow fluctuations at St = 0.22 and the helical (n = 1) flow fluctuations at St = 0.44 appear to radiate noise with substantially different efficiencies, as is evident in the following discussion.

Figure 10 has shown a hot-wire spectrum at the radial position where the St = 0.22 axisymmetric (n = 0) mode is most prevalent. Even at this position, the St = 0.44 spectral component of helical (n = ±1) mode is larger than the St = 0.22 component of axisymmetric (n = 0) mode. The spectrum in Figure 9--taken at the radial position of maximum e'_{rms}--shows that at least at some positions in the shear layer the presence of the axisymmetric (n = 0) mode at St = 0.22 is not

evident. In summary, the most predominant flow fluctuation in the shear layer is of helical ($n = \pm 1$) mode at St = 0.44 with an axisymmetric ($n = 0$) mode at St = 0.22 also present.

In the acoustic field r/D = 3.5, Figure 29 has shown the spectral component at St = 0.44 to be dominant. However, for positions of r/D greater than about 4, the St = 0.44 component is no longer present in the acoustic field. Throughout this region ($r/D > 4$), the noise spectra are quite broad with peaks at about St = 0.22 as shown in Figure 28, which is representative of spectra in this region. This St = 0.22 spectral component of the acoustic field is axisymmetric ($n = 0$), as shown in Figure 33, as is the St = 0.22 component of the flowfield, shown in Figure 23. These results strongly suggest that the axisymmetric ($n = 0$) instability component at St = 0.22 is a much more effective noise producer than the helical ($n = \pm 1$) component at St = 0.44.

Mach Number Dependence, Mach Numbers 0.90, 1.0, and 1.1 Jets

The measurements performed with the Mach number 1.0 and 1.1 jets were made to establish Mach number dependence in the transonic range. With these data any discontinuities in the transonic range could be observed on a plot of Mach number dependence.

One observation made of all three Mach numbers (0.90, 1.0, and 1.1) was the spectral content of the flow and acoustic fields. In the Mach number 1.0 jet the acoustic spectra were broad but had a peak around the same frequency as that of a dominant flowfield spectral component. This same phenomenon has also been observed in other low Reynolds

number supersonic jets by McLaughlin, Morrison, and Troutt (14, 15) and Morrison and McLaughlin (16). The hot-wire and acoustic spectra of the supersonic jets (M = 1.0 and 1.1) were shown in Figures 12 and 31 and 14 and 31, respectively.

The hot-wire spectra for the Mach number 1.1 jet had different dominant spectral components than the one seen predominantly in its acoustic field. This has not been seen in the low Reynolds number supersonic work referred to above. In this previous work, all nozzles were converging-diverging and designed for uniform parallel flow. It is therefore assumed that the difference in spectral components seen in the flow and acoustic fields of the Mach number 1.1 jet was due to the strong cell structure formed by over expanding the converging nozzle to a supersonic Mach number.

The non-dimensional frequency of the dominant spectral components of the flowfield is shown in Figure 35 for the Mach number 0.90 and 1.0 jets. On this same plot are data observed by Morrison and McLaughlin (16). This plot appears to be a continuous extension of the supersonic data. This behavior is contrary to an early theory of Tam's (28) since a frequency selection mechanism which depends on cell structure (a feature found only in supersonic jets) would not predict continuous behavior in the transonic range.

Also observed for the three Mach numbers in this study were the lengths of the potential core. This was determined in the Mach number 0.90 jet by shear layer hot-wire spectra, centerline Pitot measurements, and mean flow profiles. All three methods gave compatible results for this jet, and the shear layer hot-wire spectra were used solely for the Mach numbers 1.0 and 1.1 jets. The lengths determined are plotted in

Figure 36 as a function of Mach number along with the lengths measured by a number of other investigators. This plot indicates that the potential core lengths found in this study are consistent with those found in other studies, and none of the data give any indication of discontinuity in the transonic range.

The coherent fraction of the hot-wire signal was measured at numerous downstream locations for all three Mach numbers. These data are replotted in Figure 37 along with those obtained by Morrison (20) in low Reynolds number supersonic jets. The average coherent fraction from $x/D = 3$ to the end of the potential core is plotted in Figure 38 for each Mach number.

These data suggest that subsonic jets and supersonic jets above Mach numbers 2.5 may be the most coherent, while jets in the Mach number range from 1.1 to 2.1 may be considerably less coherent.

As reported in Chapter IV, the wavelengths were determined for various excitation frequencies in the Mach number 0.90 jet. With these known wavelengths and frequencies, the speed at which the disturbances travel downstream, c, can be calculated ($c = \lambda f$). This speed was non-dimensionalized with the mean centerline jet velocity at the nozzle exit U. The resulting non-dimensional wave speeds c/U, along with those measured in low Reynolds number supersonic jets by Morrison and McLaughlin (16) and those measured in a high Reynolds number subsonic jet by Chan (23) are presented in Table II. It can be seen in Table II that the values of c/U observed of the subsonic jet in this study are in the same range as those observed in the other jets by Morrison and Chan.

Conclusions

The Mach number 0.90 jet has large-scale coherent fluctuations in the flowfield for several diameters downstream of the nozzle exit. These fluctuations can be described by a linear instability model (the solution to the linearized instability equations for parallel flow). Two components of instability are predominant and have different azimuthal mode numbers. These are: an axisymmetric ($n = 0$) instability at $St = 0.22$ and a helical ($n = \pm 1$) instability at $St = 0.44$. The axisymmetric instability is a much more effective noise producer since the acoustic field is predominated by the same frequency and azimuthal mode number as that of the axisymmetric instability. These instabilities are very likely the dominant noise production mechanism in this low Reynolds number jet since they predominate the flow fluctuations which radiate noise of similar magnitude to that of a high Reynolds number fully turbulent jet.

The data gathered in this study indicate that the flowfield properties of low Reynolds number jets are very similar through the transonic range. However, the noise radiated from the subsonic (Mach number 0.90) jet is of an axisymmetric ($n = 0$) mode while the supersonic jets of previous studies radiated noise of helical ($n = \pm 1$) modes (15, 16). This suggests that the role of large-scale instabilities in the noise production process may be different for subsonic and supersonic jets.

BIBLIOGRAPHY

(1) Lighthill, M. J. "On Sound Generated Aerodynamically, I General Theory." Proc. Roy. Soc., A211 (1952), pp. 546-587.

(2) Lighthill, M. J. "On Sound Generated Aerodynamically, II Turbulence as a Source of Sound." Proc. Roy. Soc., A222 (1954), pp. 1-32.

(3) Ffowcs Williams, J. E. "The Noise From Turbulence Convected at High Speed." Phil. Trans. Roy. Soc., A255 (1963), p. 459.

(4) Mollo-Christensen, E. "Jet Noise and Shear Flow Instability Seen from an Experimenter's Viewpoint." Journal of Applied Mechanics, Vol. 34 (1967), pp. 1-7.

(5) Crow, S. C. and F. H. Champagne. "Orderly Structure in Jet Turbulence." J. Fluid Mech., Vol. 48 (1971), pp. 547-591.

(6) Tam, C. K. W. "Directional Acoustic Radiation From a Supersonic Jet Generated by Shear Layer Instabilities." J. Fluid Mech., Vol. 46 (1971), pp. 757-768.

(7) Laufer, J., R. E. Kaplan, and W. T. Chu. "On the Generation of Jet Noise." AGARD Conference Proceedings No. 131 on Noise Mechanisms, 1973.

(8) Lau, J. C., M. J. Fisher, and H. V. Fuchs. "The Intrinsic Structure of Turbulent Jets." Journal of Sound and Vibration, Vol. 22, No. 4 (1972), pp. 379-406.

(9) Winant, C. D. and F. K. Browand. "Vortex Pairing, the Mechanism of Turbulent Mixing Layer Growth at Moderate Reynolds Number." J. Fluid Mech., Vol. 63 (1974), pp. 237-256.

(10) Dutt, B. "Role of Large Scale Structures in the Noise Generation of a Turbulent Supersonic Jet." (Unpub. Ph.D. Thesis, University of Southern California, Los Angeles, California, 1977.)

(11) Chan. Y. Y. "Noise Generated Wavelike Eddies in a Turbulent Jet." ICAS Paper No. 76-42, 1976.

(12) Moore, C. J. "The Role of Shear-Layer Instability Waves in Jet Exhaust Noise." J. Fluid Mech., Vol. 80, Part 2 (1977), pp. 321-357.

(13) Brown, G., and Roshko, A. "The Effect of Density Difference on the Turbulent Mixing Layer." AGARD Conference on Turbulent Shear Flows, Conf. Proc. No. 93, p. 23, 1971.

(14) McLaughlin, D. K., G. L. Morrison, and T. R. Troutt. "Experiments on the Instability Waves in a Supersonic Jet and Their Acoustic Radiation." J. Fluid Mech., Vol. 69 (1976), pp. 73-95.

(15) McLaughlin, D. K., G. L. Morrison and T. R. Troutt. "Reynolds Number Dependence in Supersonic Jet Noise." AIAA J., Vol. 15 (1977), pp. 526-532.

(16) Morrison, G. L. and McLaughlin, D. K. "The Instability Process in Low Reynolds Number Supersonic Jets." Submitted for publication, J. of Fluid Mechanics, March, 1978.

(17) Smith, R. H. and Chi-Teh Wang. "Contracting Cones Giving Uniform Throat Speeds." J. of the Aeronautical Sciences, 1974, pp. 356-360.

(18) Kendall, J. M. "Supersonic Boundary Layer Stability Experiments." Proc. of the Boundary Layer Transition Study Group Meeting, Vol. II, Aerospace Report No. TR-0158 (S3816-63)-1, 1967.

(19) Wooley, J. P. and Karamcheti, K. "The Role of Jet Stability in Edgetone Generation." AIAA Paper No. 73-628, 1973.

(20) Morrison, G. L. "Flow Instability and Acoustic Radiation Measurements of Low Reynolds Number Supersonic Jets." (Unpub. Ph.D. Thesis, Oklahoma State University, Stillwater, Oklahoma, 1977.)

(21) Horstman, C. C., and Rose, W. C. "Hot-Wire Anemometry in Transonic Flow." AIAA J., Vol. 15, No. 3 (1977), pp. 395-401.

(22) Mollo-Christensen, E., Kolpin, M. A., and Martucelli, J. R. "Experiments on Jet Flows and Jet Noise Far-Field Spectra and Directivity Patterns." J. Fluid Mech., Vol. 18, Part 2 (1964), pp. 285-301.

(23) Chan, Y. Y. "Spatial Waves in Turbulent Jets." The Physics of Fluids, Vol. 17, No. 1 (1974), pp. 46-53.

(24) Dahan, C. and Elias, G. "Source Structure Pattern in a Hot Jet by Infrared-Microphones Correlations." AIAA Paper No. 76-542, 1976.

(25) McLaughlin, D. K. "Experimental Investigation of the Stability of the Laminar Supersonic Cone Wake." AIAA, Vol. 9, No. 4 (1971), pp. 696-702.

(26) Morris, P. J. and Tam, C. K. W. "Near and Far/ Field Noise from Large-Scale Instabilities of Axisymmetric Jets." AIAA Paper No. 77-1351, 1977.

(27) Michalke, A. and Fuchs, H. V. "On Turbulence and Noise of an Axisymmetric Shear Flow." J. Fluid Mech., Vol. 70 (1975), pp. 179-205.

(28) Tam, C. K. W. "On the N ise of a Nearly Ideally Expanded Supersonic Jet." J. Fluid Mech., Vol. 51 (1972), pp. 69-95.

(29) Lau, J. C., P. J. Morris, and M. J. Fisher. "Turbulence Measurements in Subsonic Jets Using a Laser Lelocimeter." AIAA Paper No. 76-348, 1976.

(30) Knott, P. et al. "Laser Velcimeter Developments for Noise Source Location." Air Force Aero Propulsion Lab. TR-(To be assigned), Vol. II, Chapter 3, August, 1975.

(31) Morris, P. J. "Turbulence Measurements in Subsonic and Supersonic Axisymmetric Jets in a Moving Stream." AIAA Paper No. 76-25, 1976.

(32) Nagamatsu, H. T. and R. E. Sheer, Jr. "Subsonic and Supersonic Jets and Supersonic Supressor Characteristics." AIAA Paper No. 73-999, 1973.

(33) Morkovin, M. V. Fluctuations and Hot-Wire Anemometry in Compressible Fluids. AGARDograph No. 24, Paris: NATO, November, 1956.

(34) Kovasznay, L. S. G. "The Hot-Wire Anemometer in Supersonic Flow." J. Aero. Sci., Vol. 17, No. 9 (Sept., 1950), pp. 565-572.

(35) Ko, C. L., D. K. McLaughlin and T. R. Troutt. "Improved Techniques for Hot-Wire Fluctuation Measurements in Supersonic Flows." AIAA Paper No. 76-398, 1976.

(36) Rose, W. C. "The Behavior of a Compressible Turbulent Boundary Layer in a Shock-Wave-Induced Adverse Pressure Gradient." NASA TN D-7092, 1973.

APPENDIX A

HOT-WIRE DATA REDUCTION TECHNIQUE

Morkovin (33) and Kovasznay (34) have established that the fluctuating voltage of a heated wire may be expressed as:

$$\frac{E'}{\overline{E}} = A_\rho \frac{\rho'}{\overline{\rho}} + A_u \frac{u'}{\overline{u}} + A_T \frac{T_o'}{\overline{T}_o}$$

where A_ρ, A_u, and A_T are the sensitivey coefficients for density, velocity, and total temperature fluctuations, respectively. In supersonic jets with similar temperature conditions Ko et al. (35) established that fluctuations in total temperature are small and have a negligible influence on the hot-wire measurements. Consequently the total temperature fluctuation term was also assumed to be negligible in the present experiments.

The velocity sensitivity coefficient A_u was determined by measuring the mean voltage $\overline{E}$ for numerous values of velocity while the density remained constant. These measurements were made for incremental values of constant density between $0.590\rho_t$ (the ambient density ρ_o at Mach number 0.90) and $0.681\rho_t$ (the centerline density at Mach number 0.90). The plot for $\rho = 1.42 \times 10^3$ lb_m/ft^3 is shown in Figure 39 for four values of hot-wire resistance over-heat $a_w = \frac{R_w - R_{aw}}{R_{aw}}$. From this plot the velocity sensitivity coefficient was determined by

$$A_u = \frac{u}{\overline{E}} \frac{\partial \overline{E}}{\partial u} \Bigg|_{\rho = \text{const.},\ T_o = \text{const.}}$$

In a similar manner the density sensitivity coefficient A_ρ was determined by measuring the mean voltage $\overline{E}$ for numerous values of density while the velocity remained constant. These measurements were made for incremental values of constant velocity up to 943 ft/sec (the centerline

velocity at Mach number 0.90). The plot for u = 850 ft/sec is shown in Figure 40 for the same overheats as those in Figure 39. From this plot the density sensitivity coefficient was determined by

$$A_\rho = \frac{\rho}{\overline{E}} \left.\frac{\partial \overline{E}}{\partial \rho}\right|_{u = \text{const.},\ T_o = \text{const.}}$$

To decompose the hot-wire voltage into density and velocity fluctuations, the corresponding sensitivities were calculated from the appropriate curves in the following manner: The mean flow profiles (Figure 7) were used to determine the mean velocity $\overline{V}$ at the location of the hot wire. A_ρ was then calculated as discussed above from the plot of density ρ versus mean hot-wire voltage $\overline{E}$ at this constant velocity $\overline{V}$. A_u was assumed to be negligible since, as shown in Figure 39, the plots of u versus $\overline{E}$ indicate that the hot-wire output voltage has only a weak dependence on velocity.

This unusual behavior is a consequence of the heat loss from the hot-wire being dominated by conduction end-loss heat transfer. The conduction end-loss problem associated with hot-wire fluctuation measurements in supersonic flows has been analyzed by Rose (36) and Ko et al. (35). However, very little published information is currently available on hot-wire fluctuation measurements in the transonic flow regime at very low Reynolds numbers.

APPENDIX B

TABLES

TABLE I

INSTABILITY CHARACTERISTICS

Mach Number M	Component of Instability St	Growth Rate $-k_i D$	Wave Number $k_r D$	Azimuthal mode Number n
Present Measurements				
0.90	0.22	1.7	2.03	0
0.90	0.44	2.1	4.34	±1
0.90	0.55	---	4.91	---
0.90	0.69	---	6.51	---
Measurements of Chan (23)				
0.19	0.20	1.5	1.6	---
0.19	0.44	3.7	4.2	---
Measurements of Morrison and McLaughlin (16)				
1.4	0.33	0.81	3.43	±1
2.1	0.22	0.59	2.37	±1
2.5	0.16	0.32	1.50	±1

TABLE II

WAVE SPEEDS OF SUBSONIC AND SUPERSONIC JETS

Mach Number	St	c/U
Measurements of Chan (23)		
0.19	0.35	0.65
0.19	0.50	0.60
Present Measurements		
0.90	0.22	0.68
0.90	0.44	0.64
0.90	0.55	0.70
0.90	0.69	0.66
Measurements of Morrison and McLaughlin (16)		
1.4	0.33	0.61
2.1	0.22	0.58
2.5	0.14	0.69
2.5	0.16	0.67
2.5	0.18	0.68

APPENDIX C

FIGURES

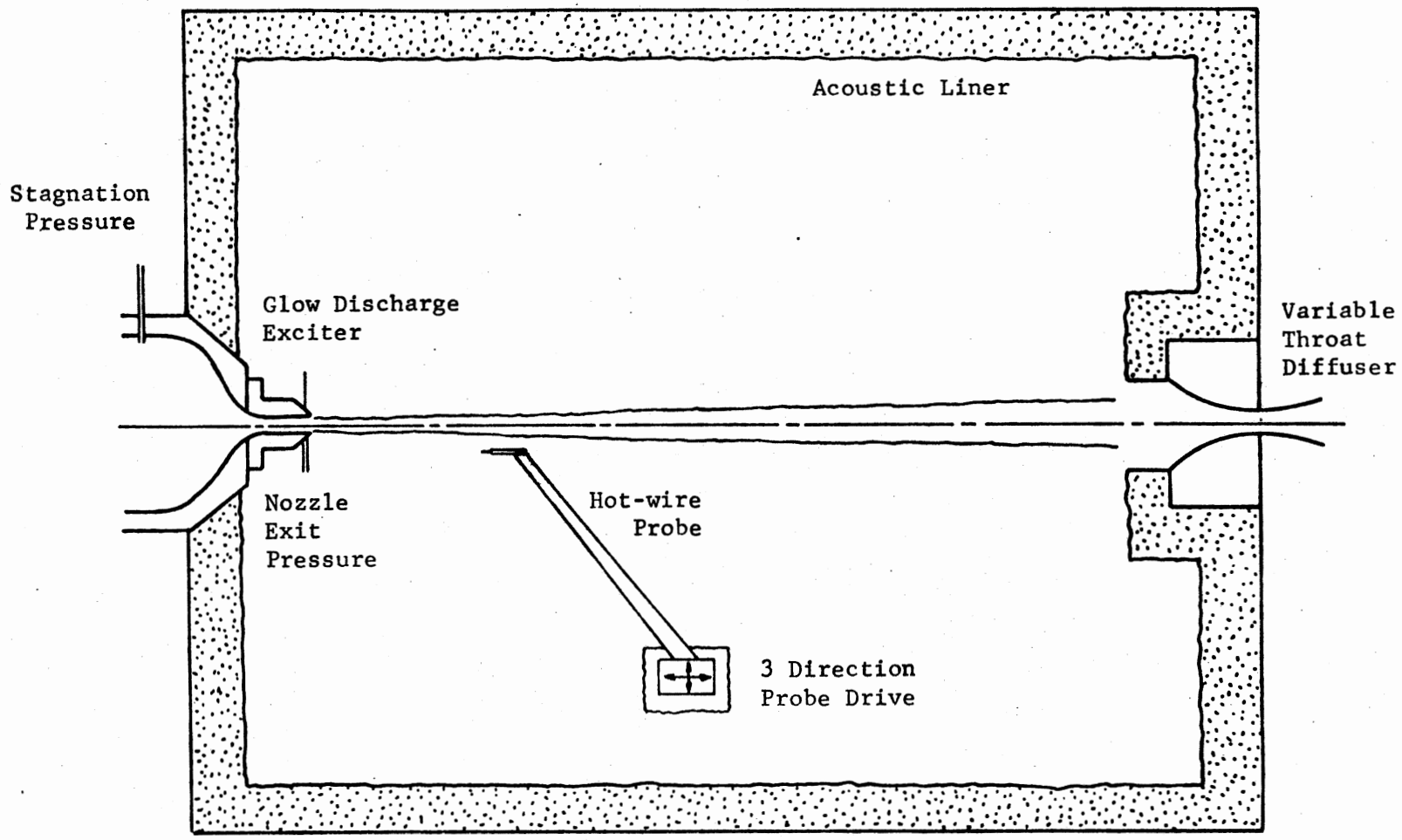

Figure 1. Schematic Diagram of Jet Test Chamber

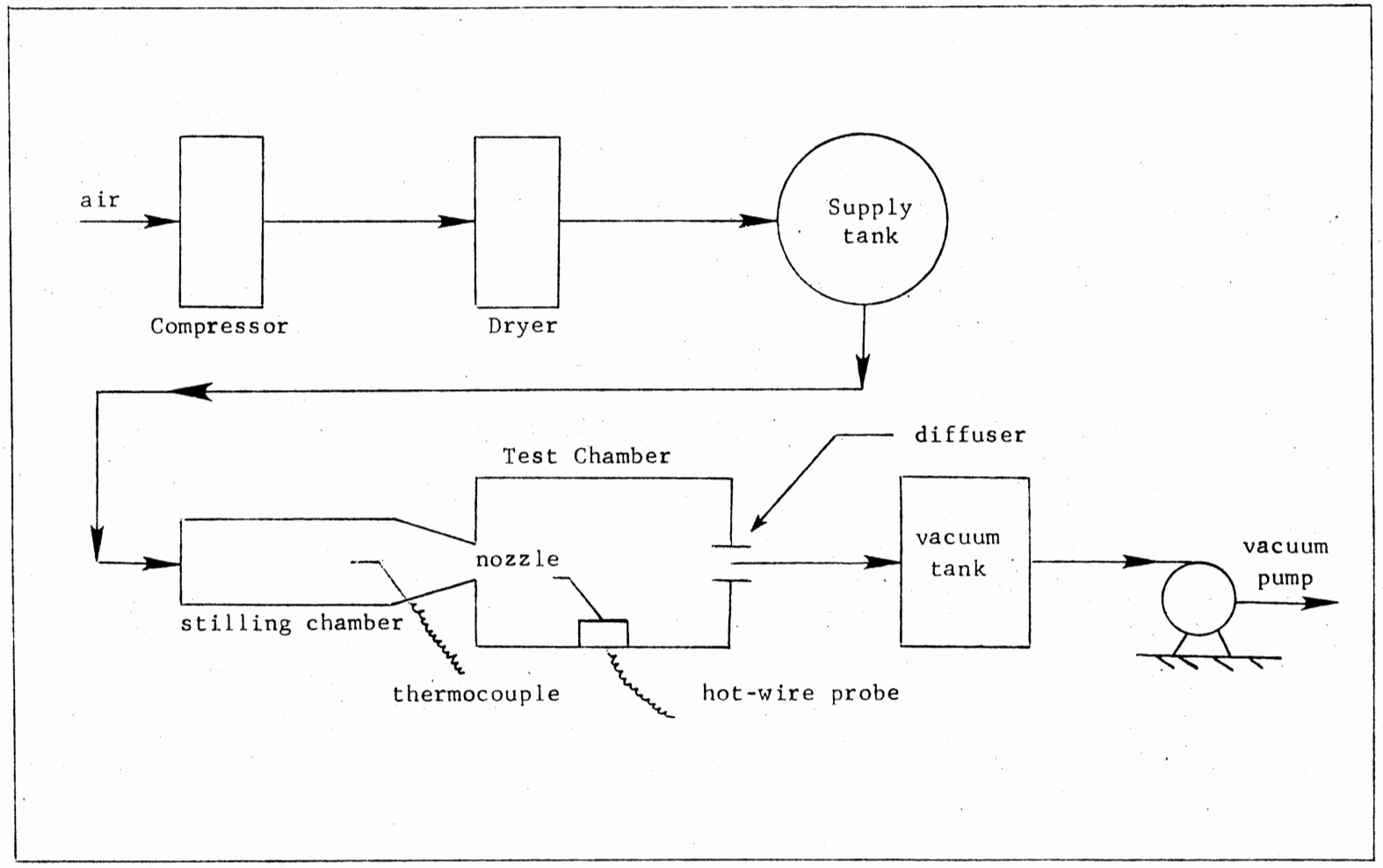

Figure 2. Schematic Diagram of Complete Facility

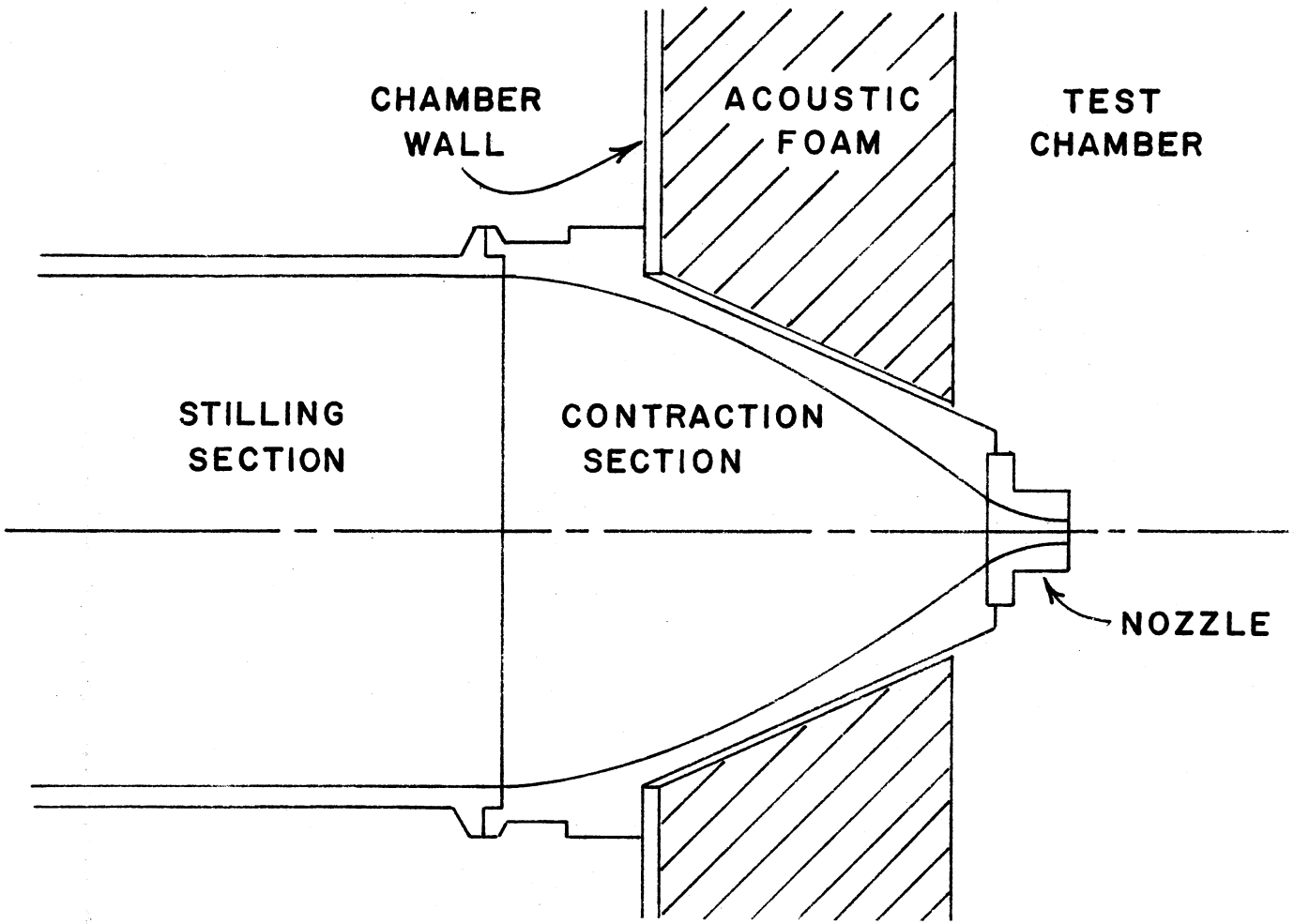

Figure 3. Schematic Diagram of Stilling Section, Contraction Section, and Nozzle

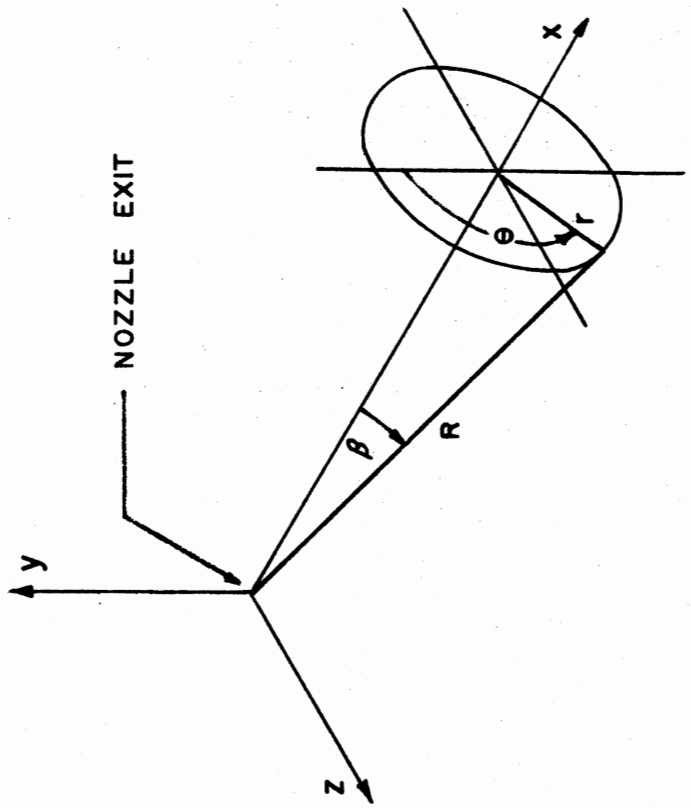

Figure 4. Facility Coordinate System

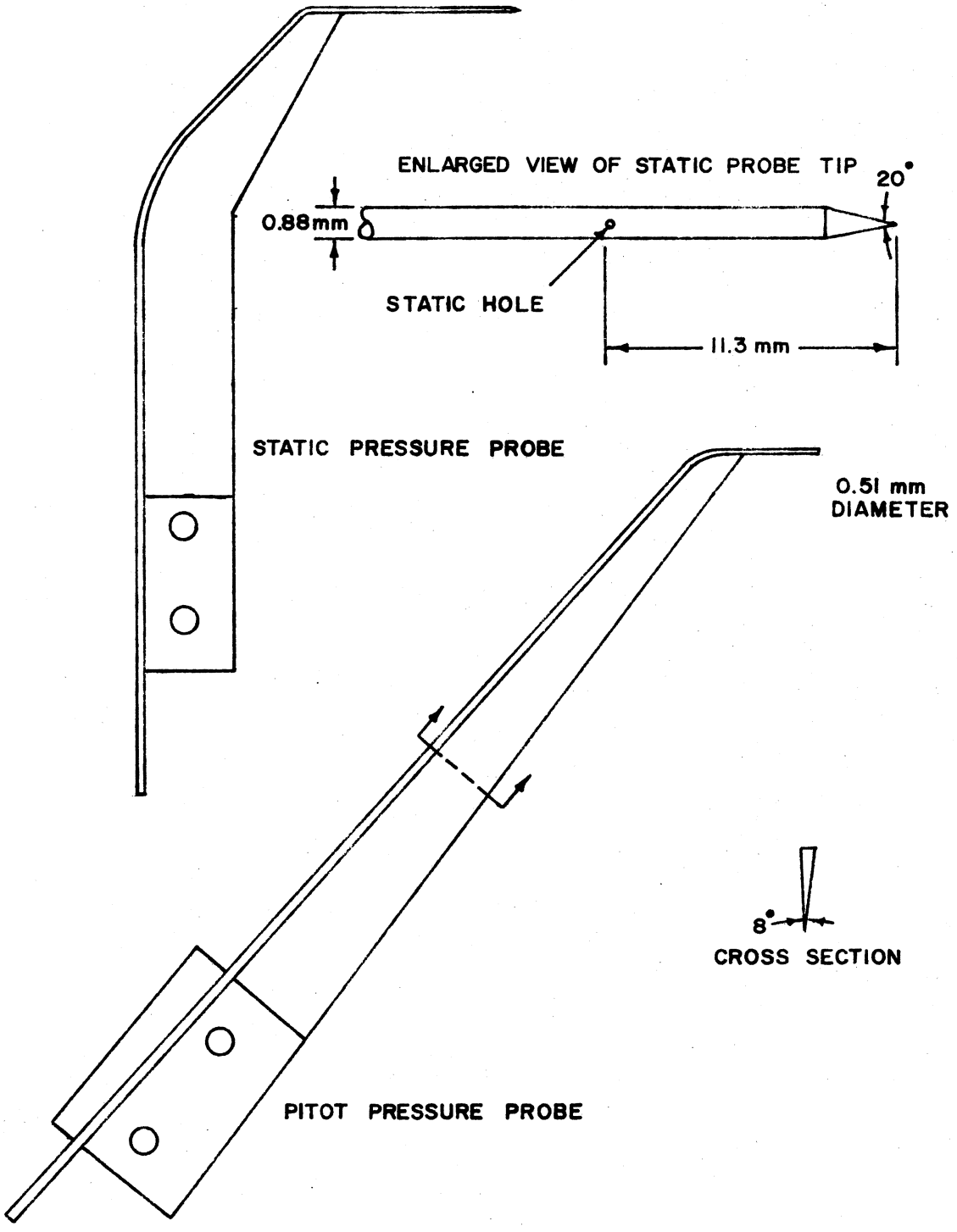

Figure 5. Static Pressure and Pitot Pressure Probes

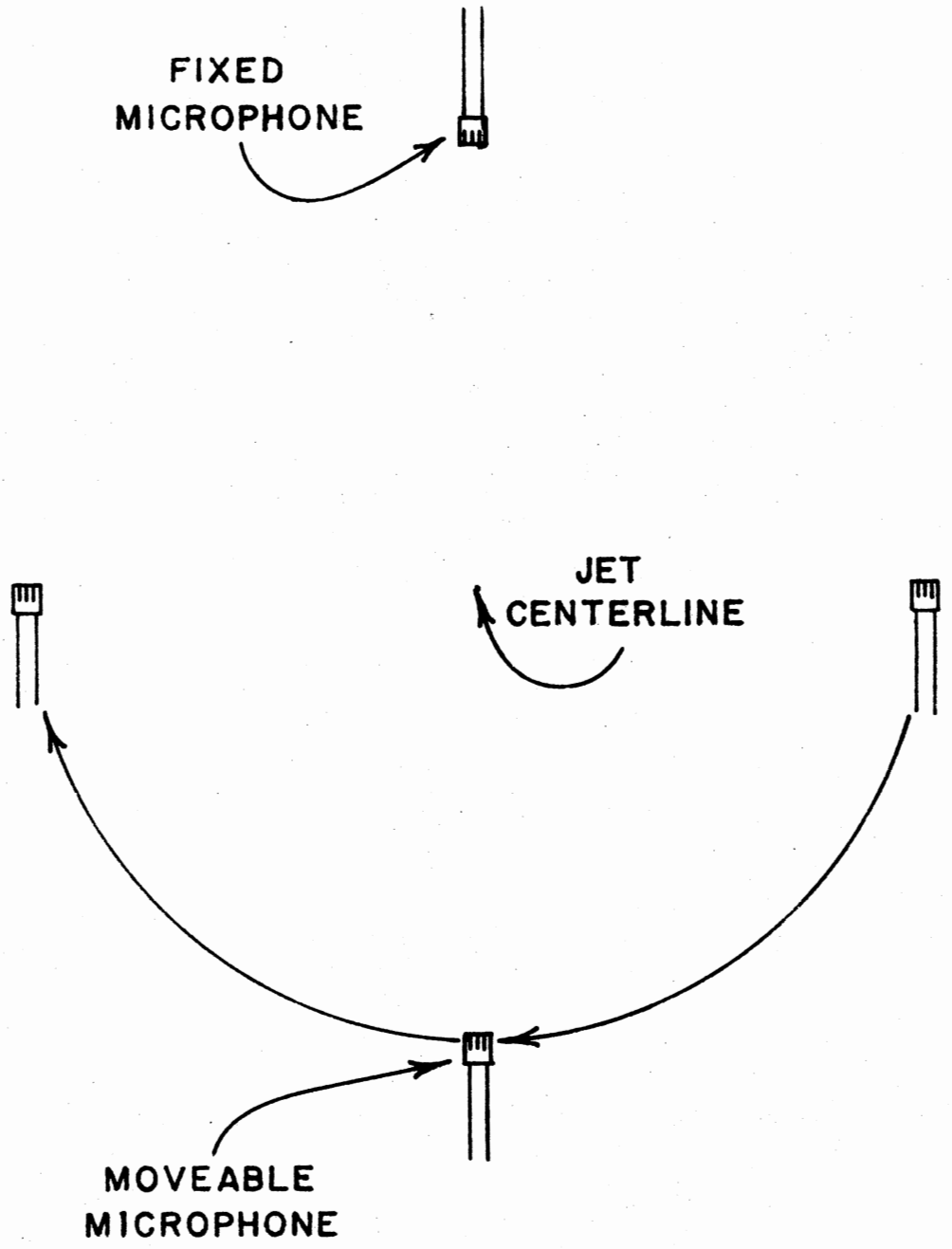

Figure 6. Microphone Setup for Azimuthal Phase Measurements

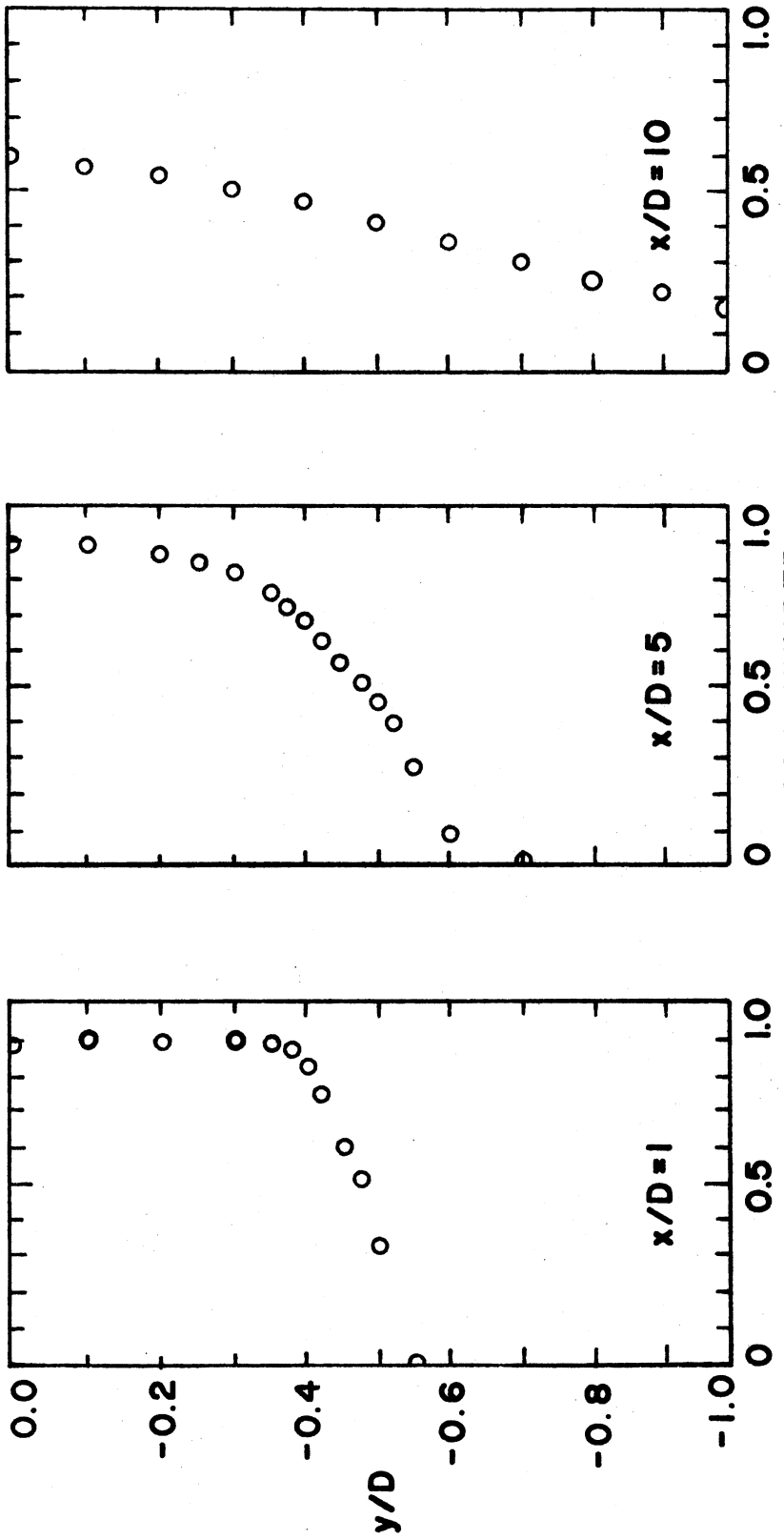

Figure 7. Mean Flow, Mach Number 0.90

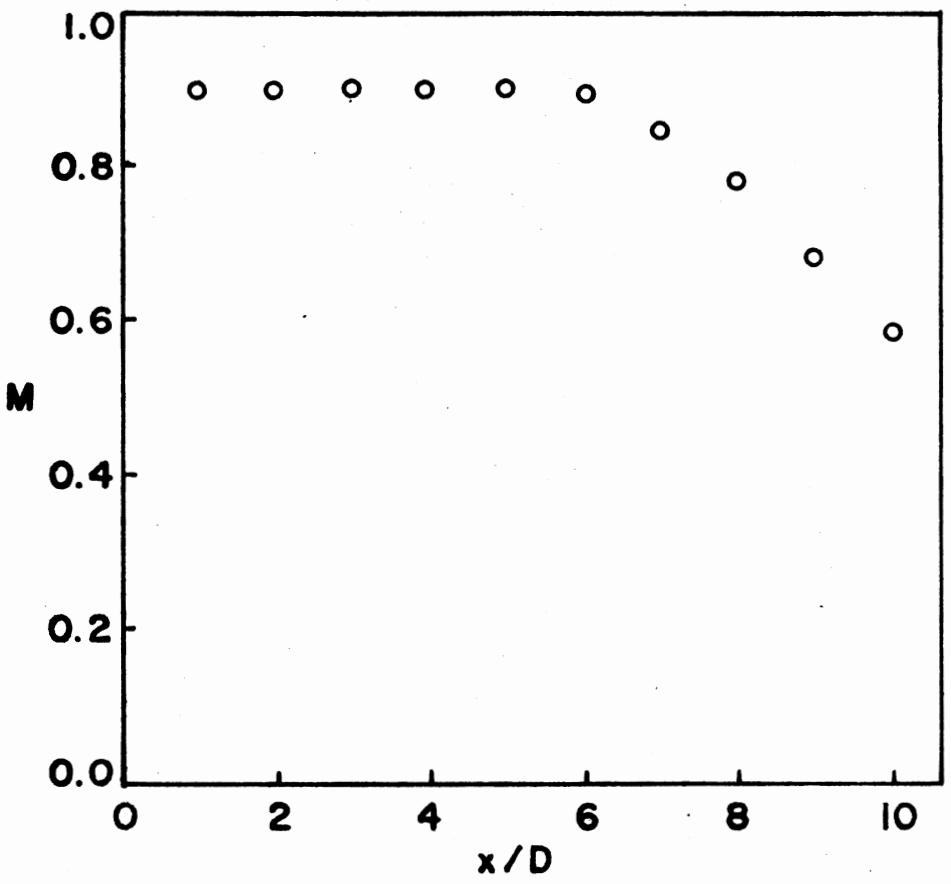

Figure 8. Axial Distribution of Centerline Mach Number

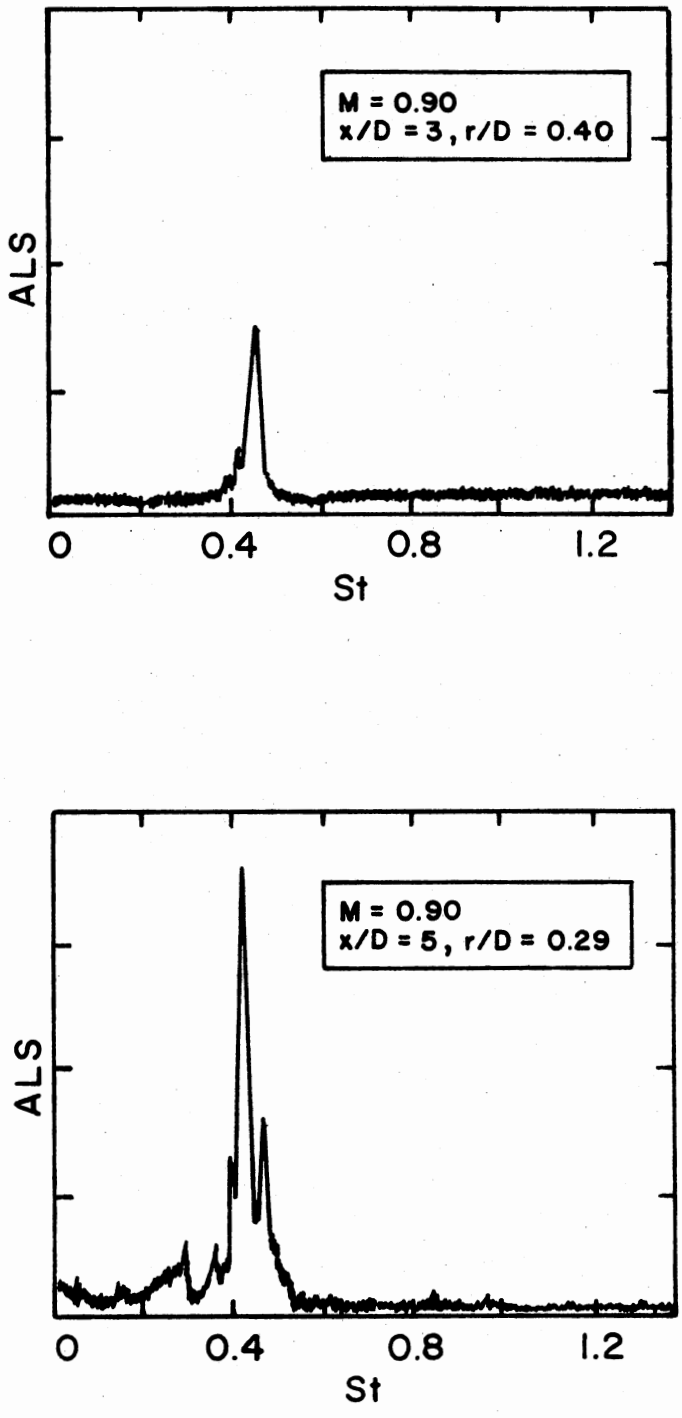

Figure 9. Hot-Wire Spectra, Mach Number 0.90

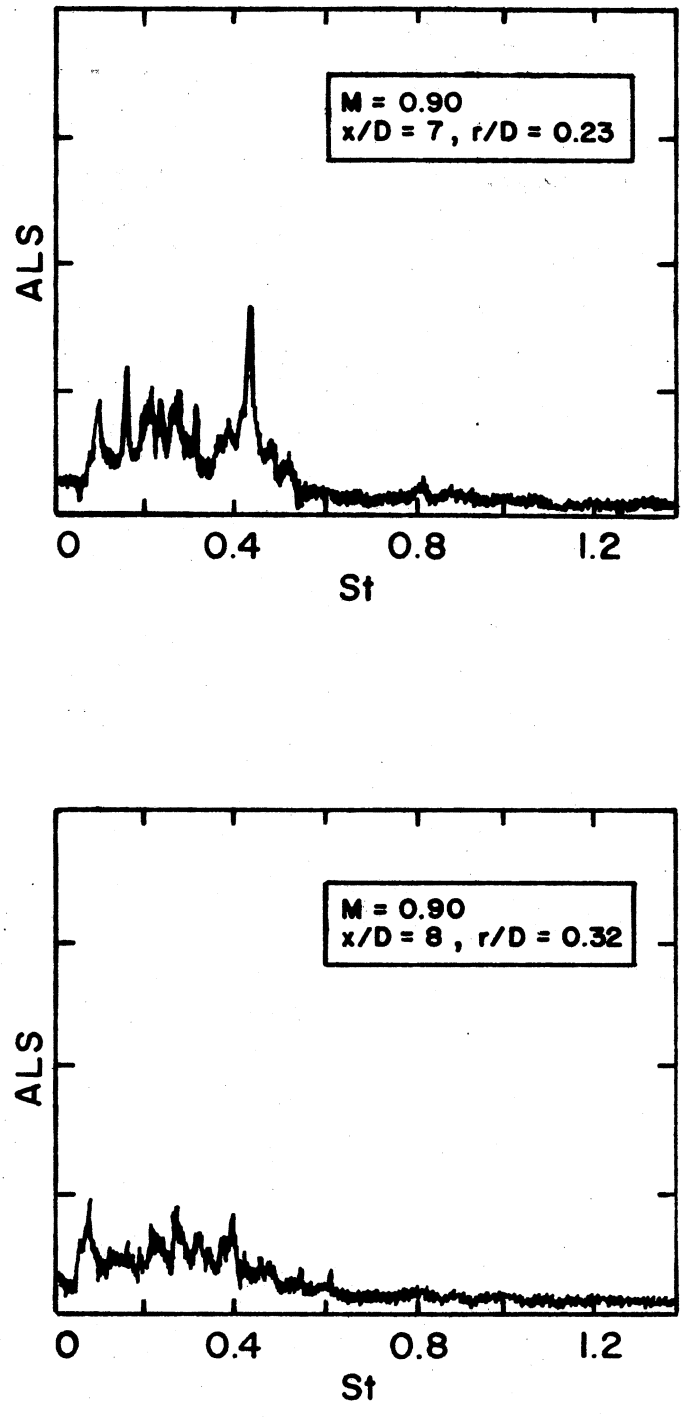

Figure 9. (Continued)

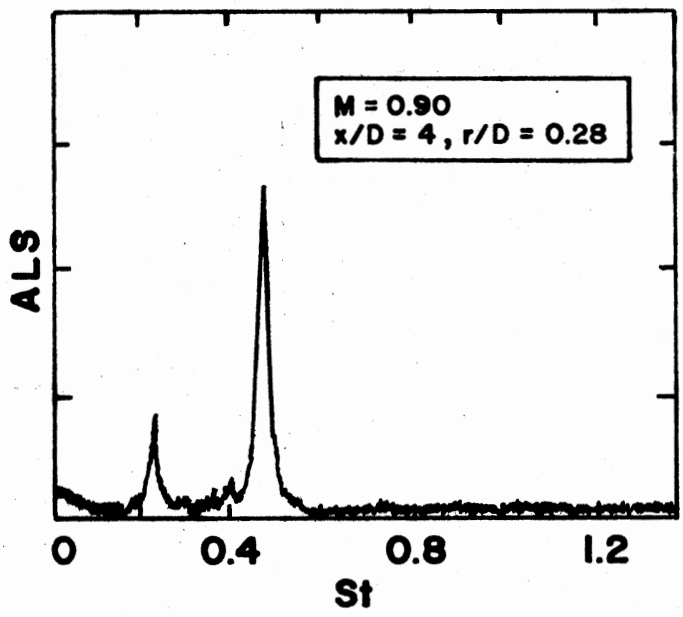

Figure 10. Hot-Wire Spectrum, Mach Number 0.90

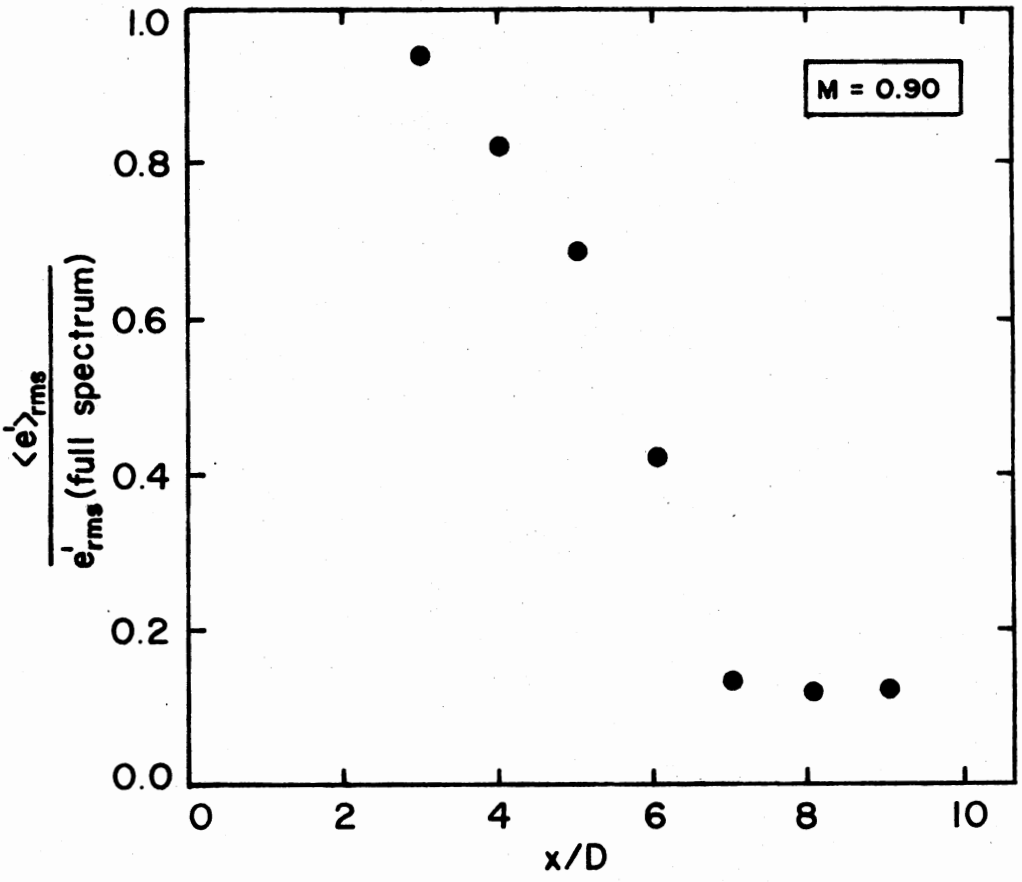

Figure 11. Fraction Coherence of Hot-Wire Signal, Mach Number 0.90

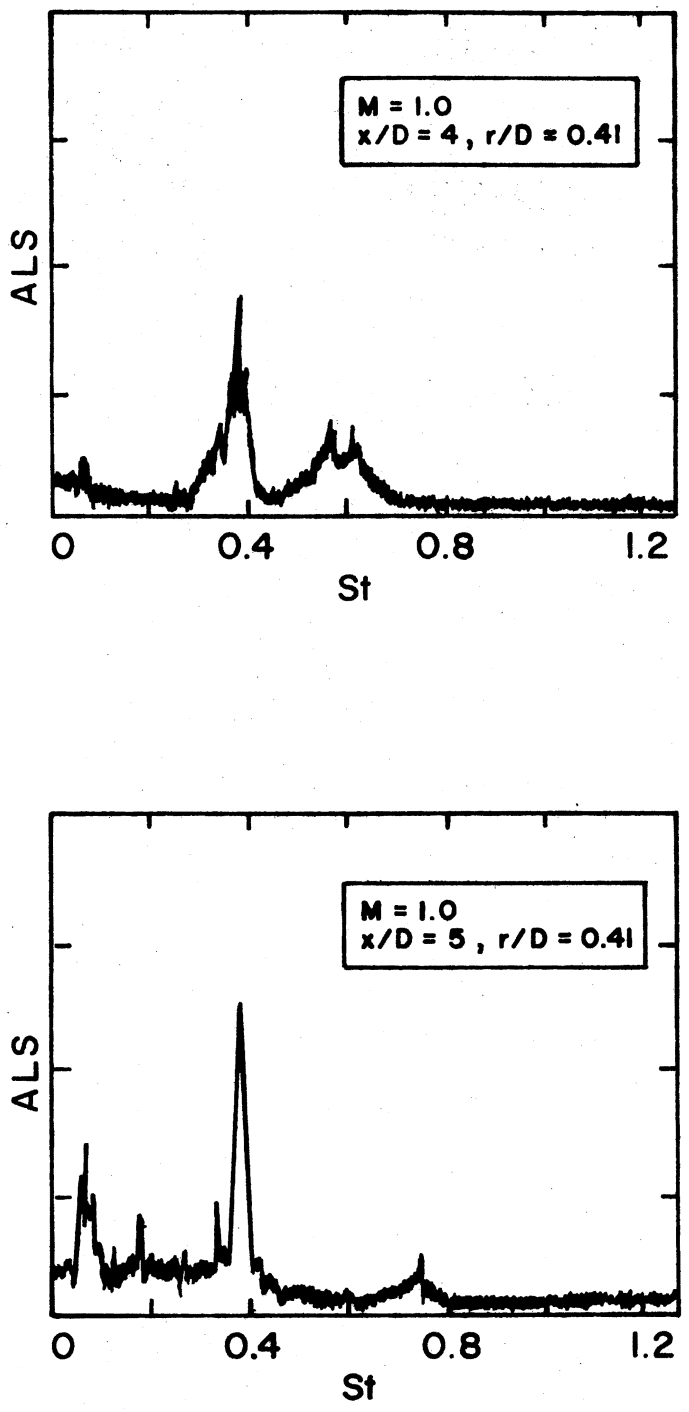

Figure 12. Hot-Wire Spectra, Mach Number 1.0

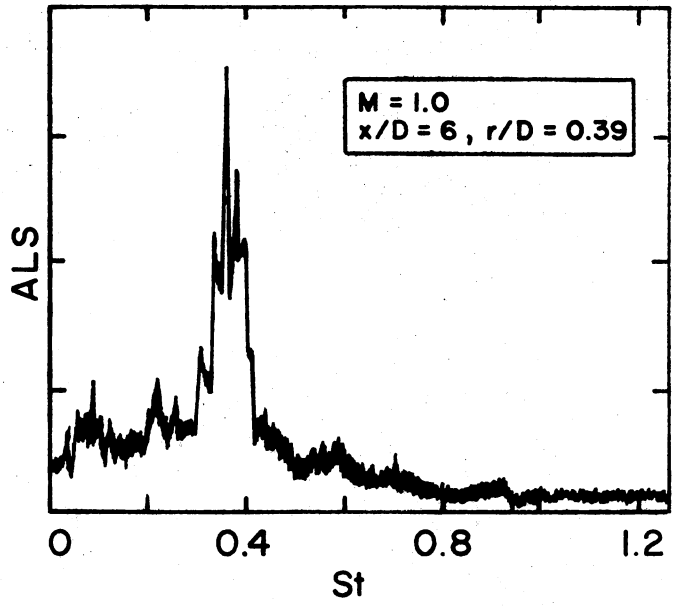

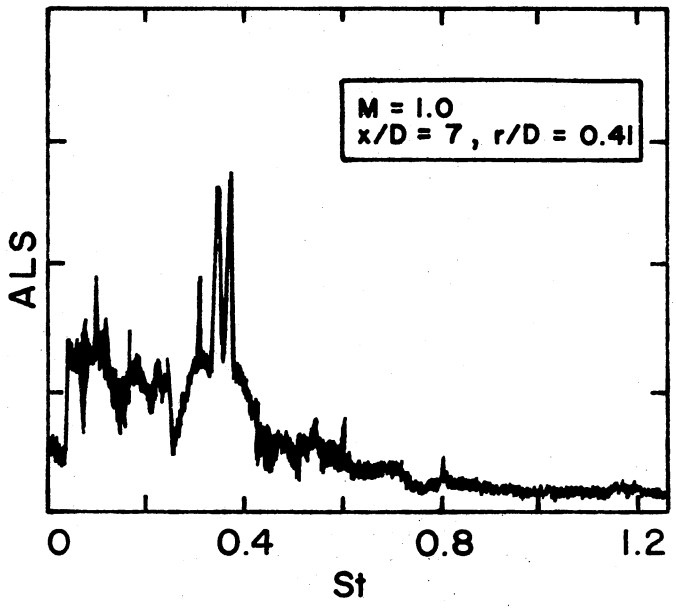

Figure 12. (Continued)

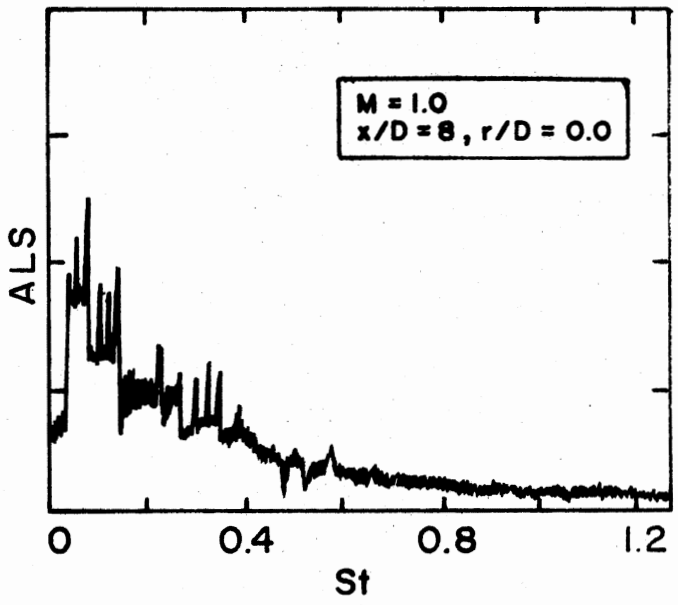

Figure 12. (Continued)

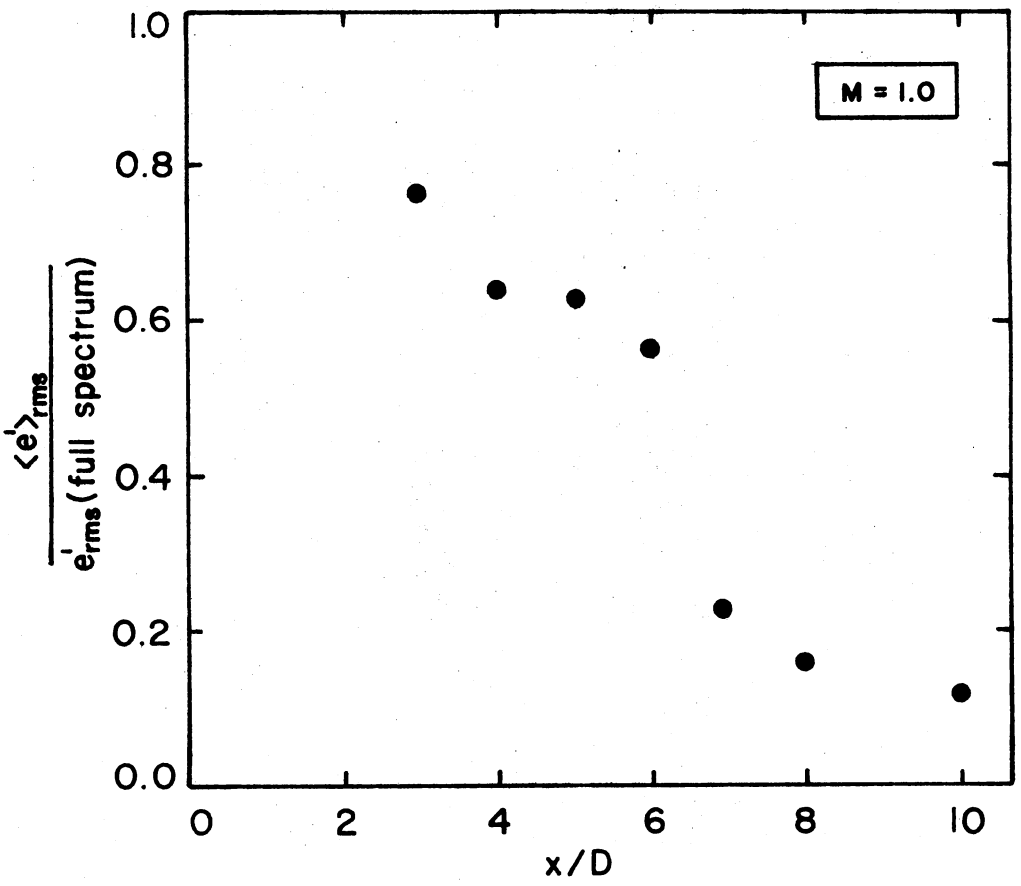

Figure 13. Fraction Coherence of Hot-Wire Signal, Mach Number 1.0

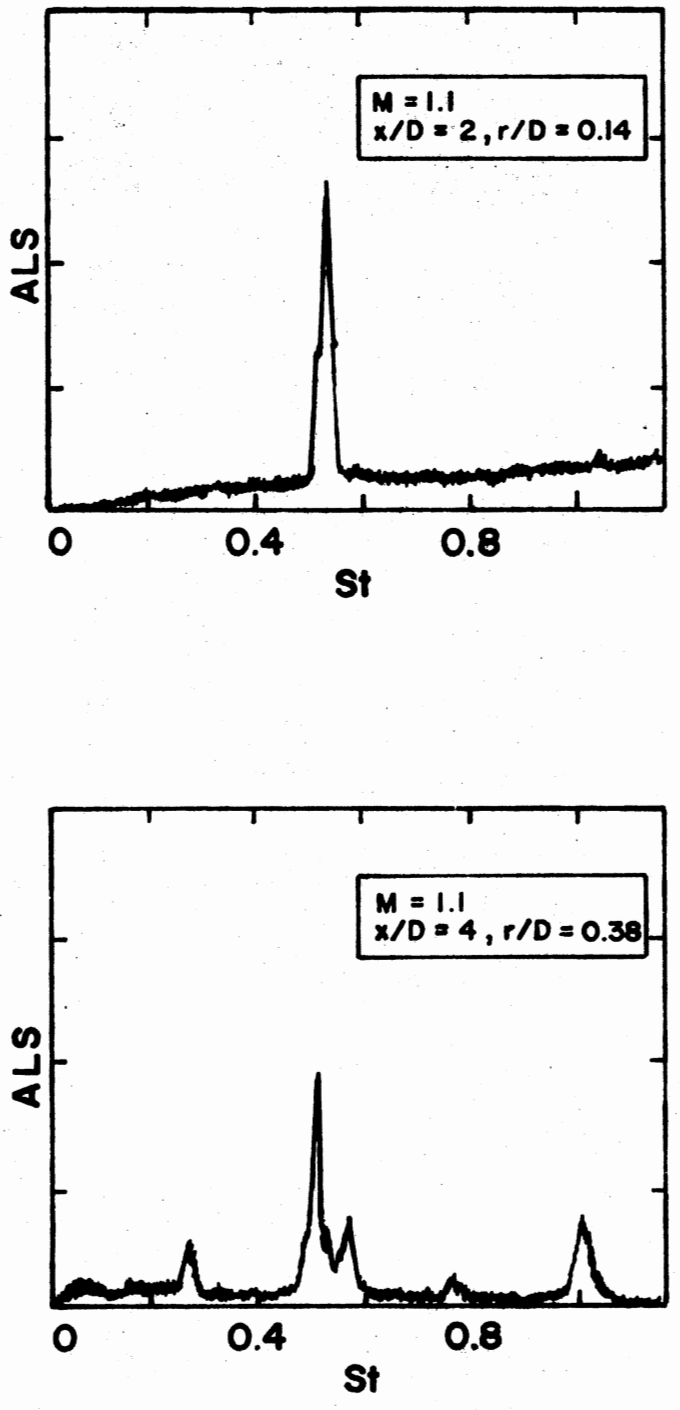

Figure 14. Hot-Wire Spectra, Mach Number 1.1

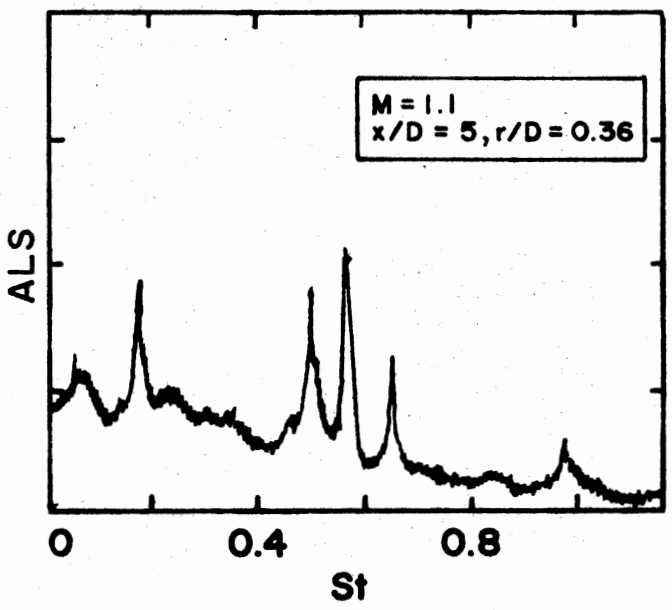

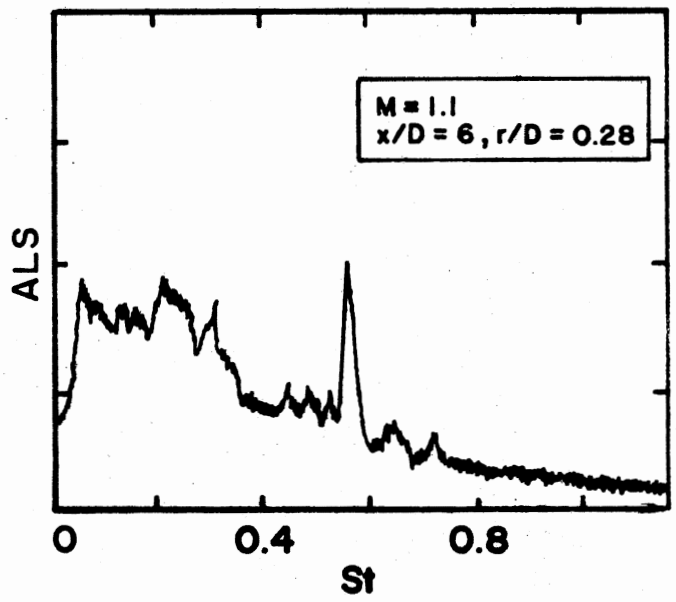

Figure 14. (Continued)

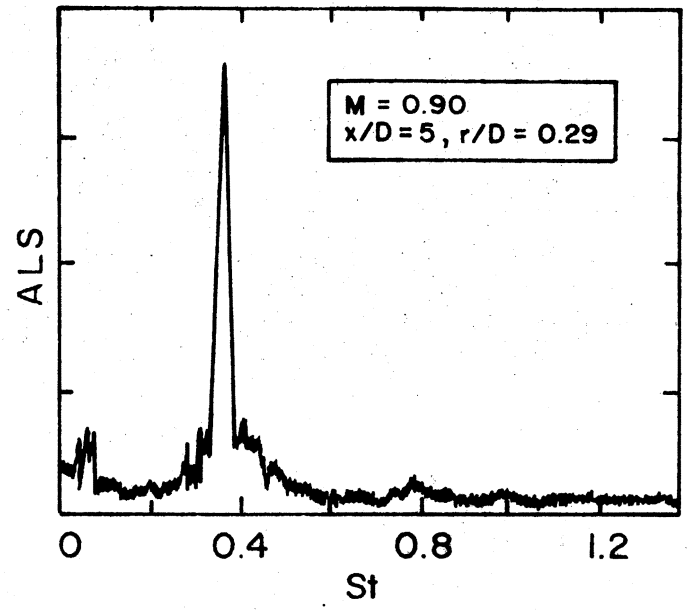

Figure 15. Hot-Wire Spectrum of Mach Number 0.90 Jet Excited at St = 0.38

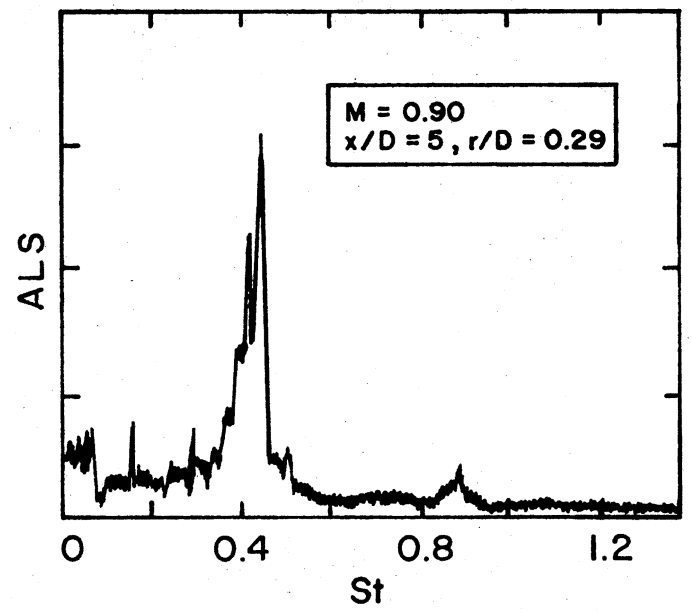

Figure 16. Hot-Wire Spectrum of Natural Jet, Mach Number 0.90

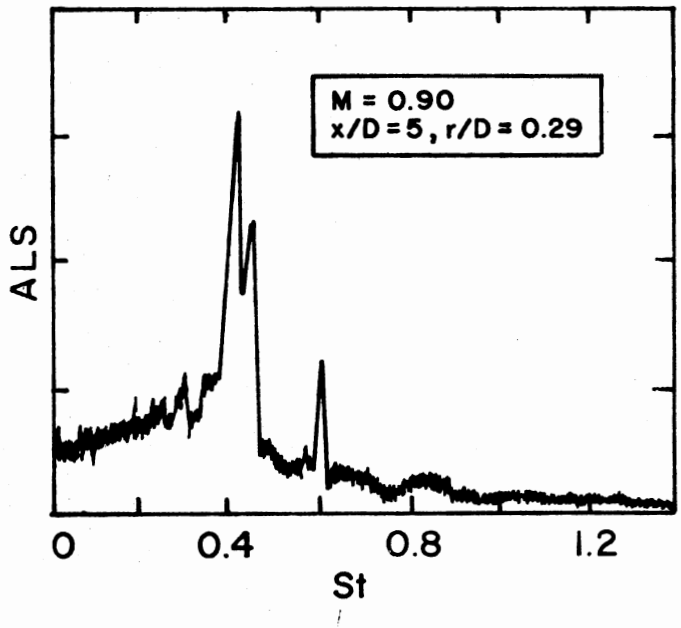

Figure 17. Hot-Wire Spectrum of Mach Number 0.90 Jet Excited at St = 0.60

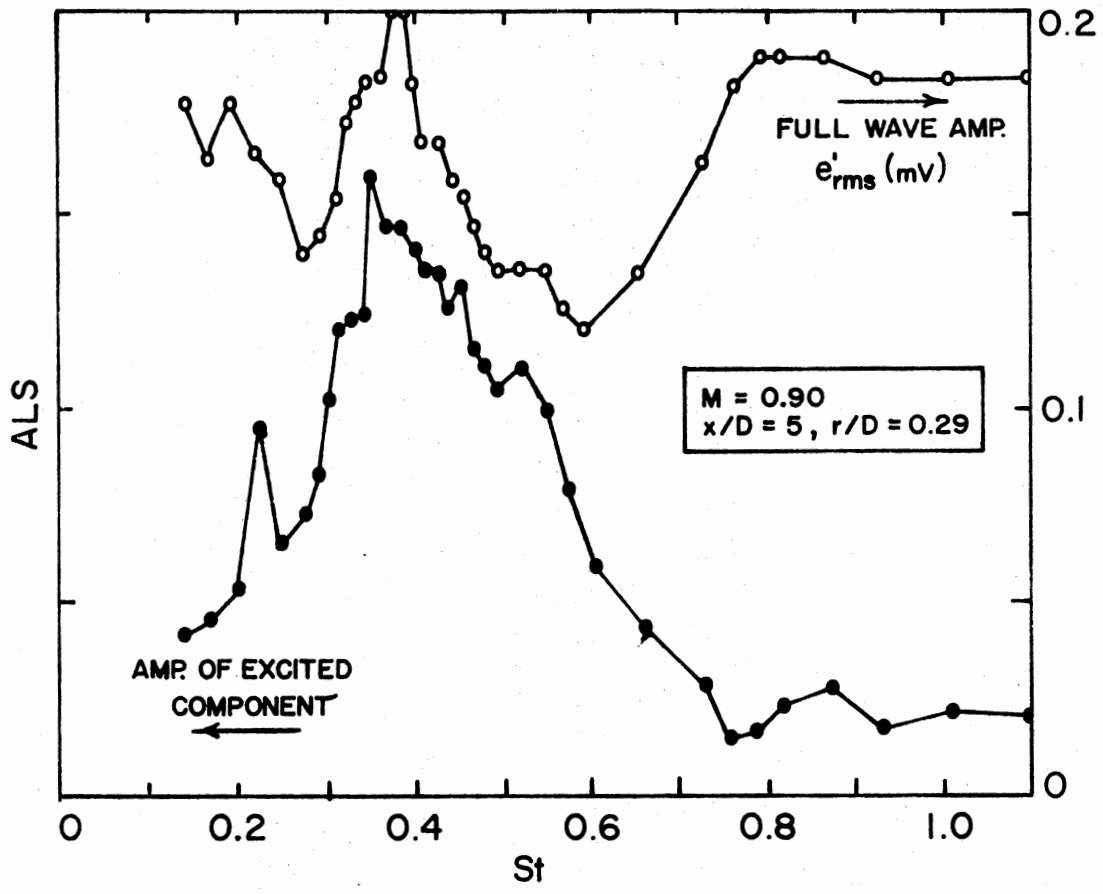

Figure 18. Flowfield Response to Excitation, Mach Number 0.90

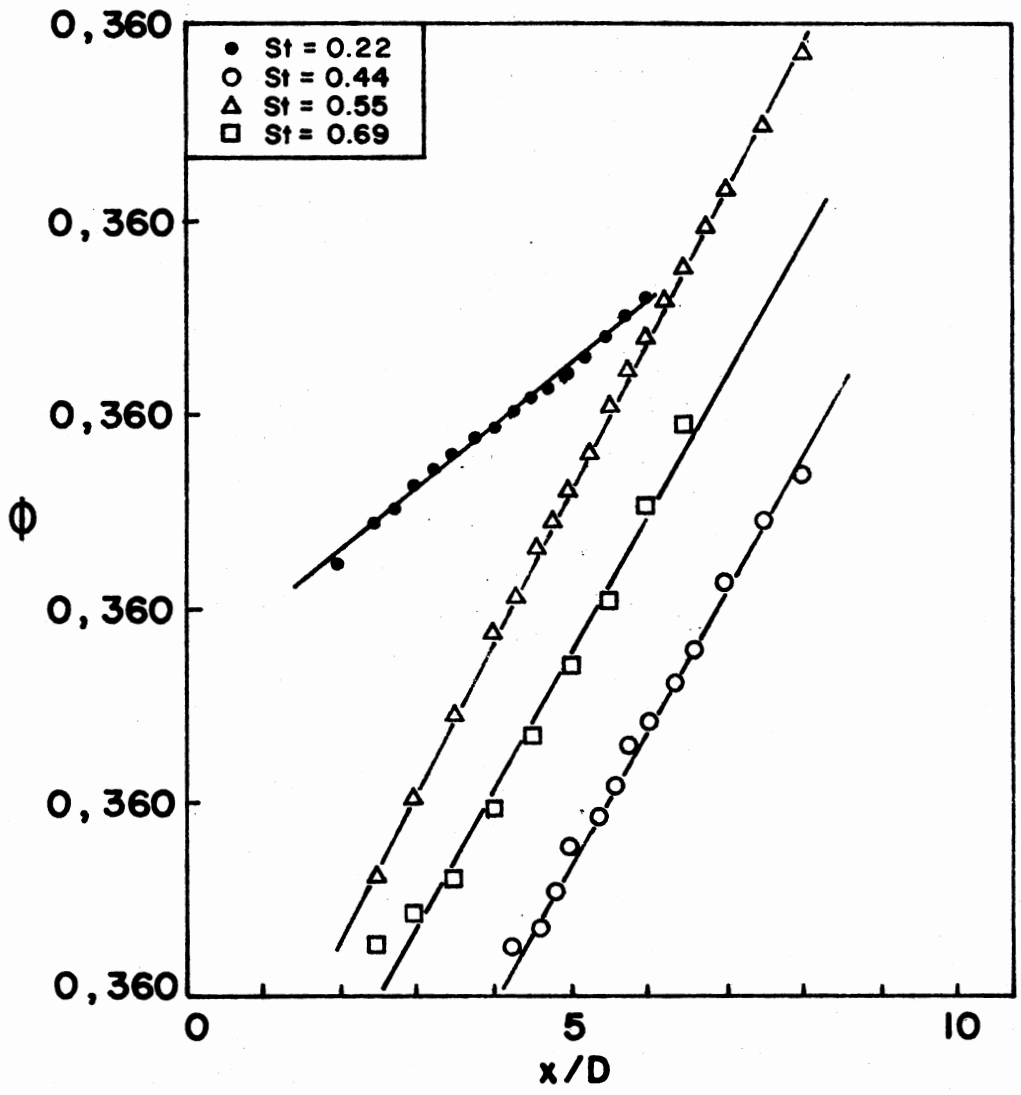

Figure 19. Axial Phase Distributions of Spectral Components, Mach Number 0.90

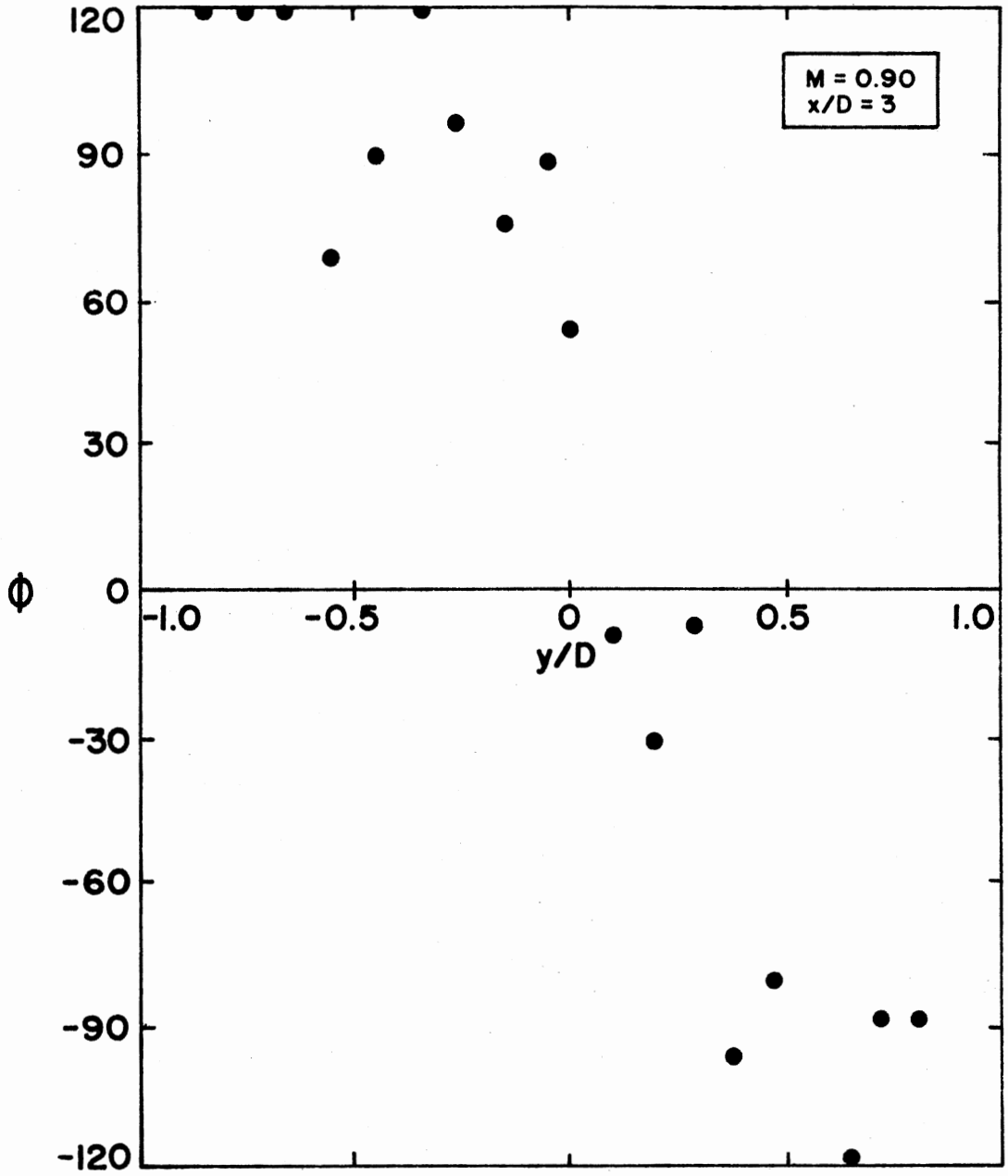

Figure 20. Distribution of Radial Phase (Flowfield), St = 0.44 Component, Mach Number 0.90

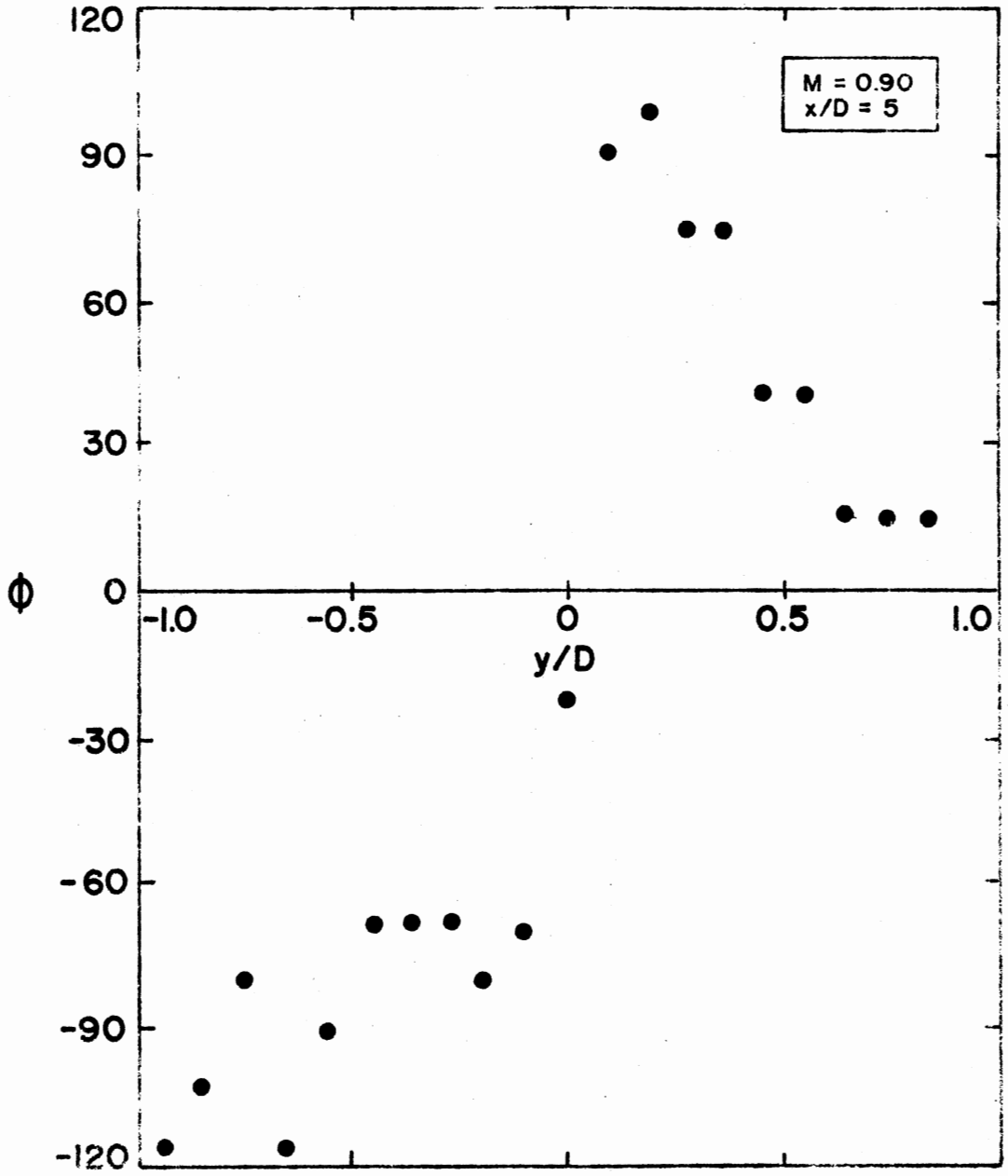

Figure 20. (Continued)

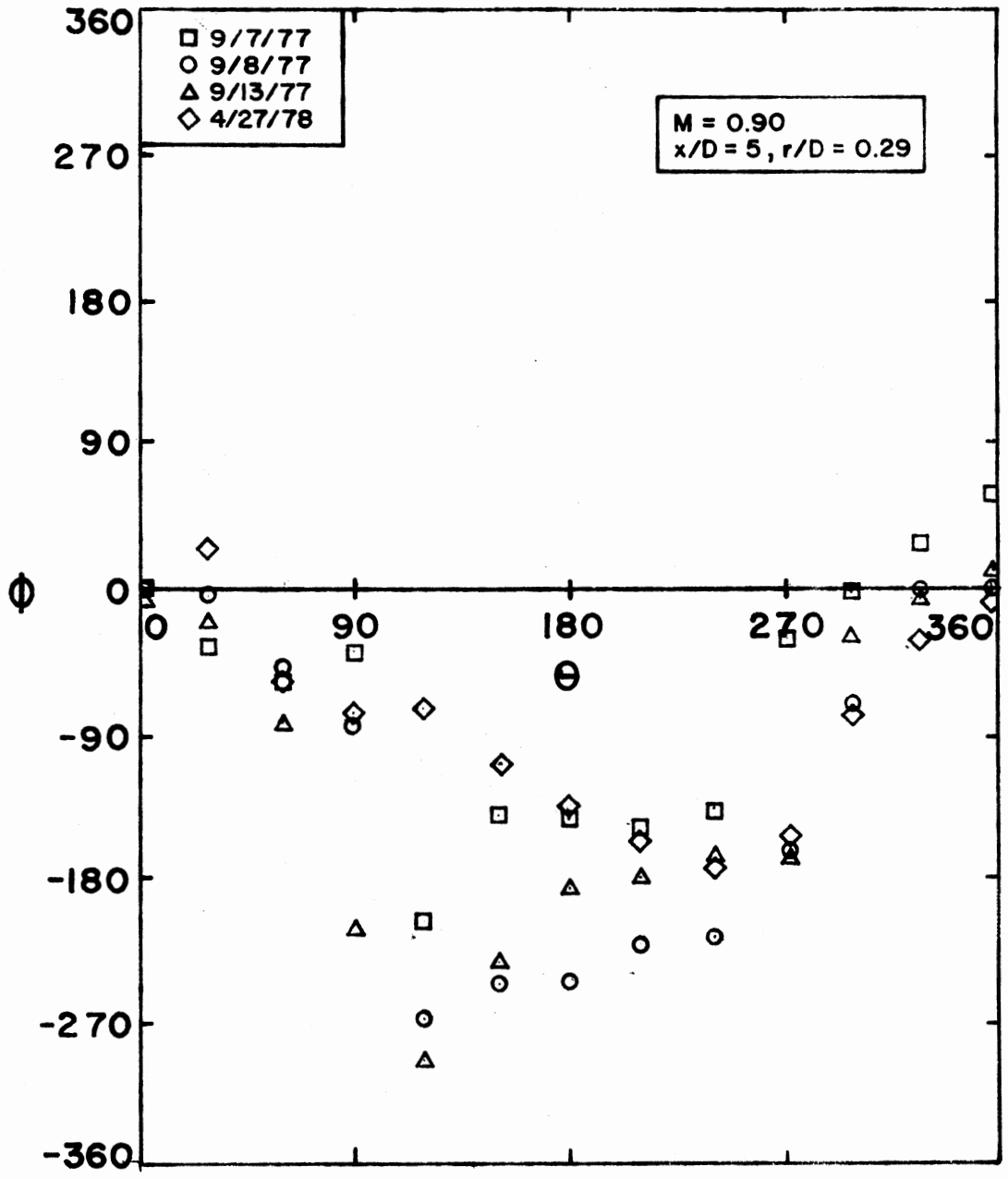

Figure 21. Distribution of Azimuthal Phase (Flowfield), St = 0.44 Component, Mach Number 0.90.

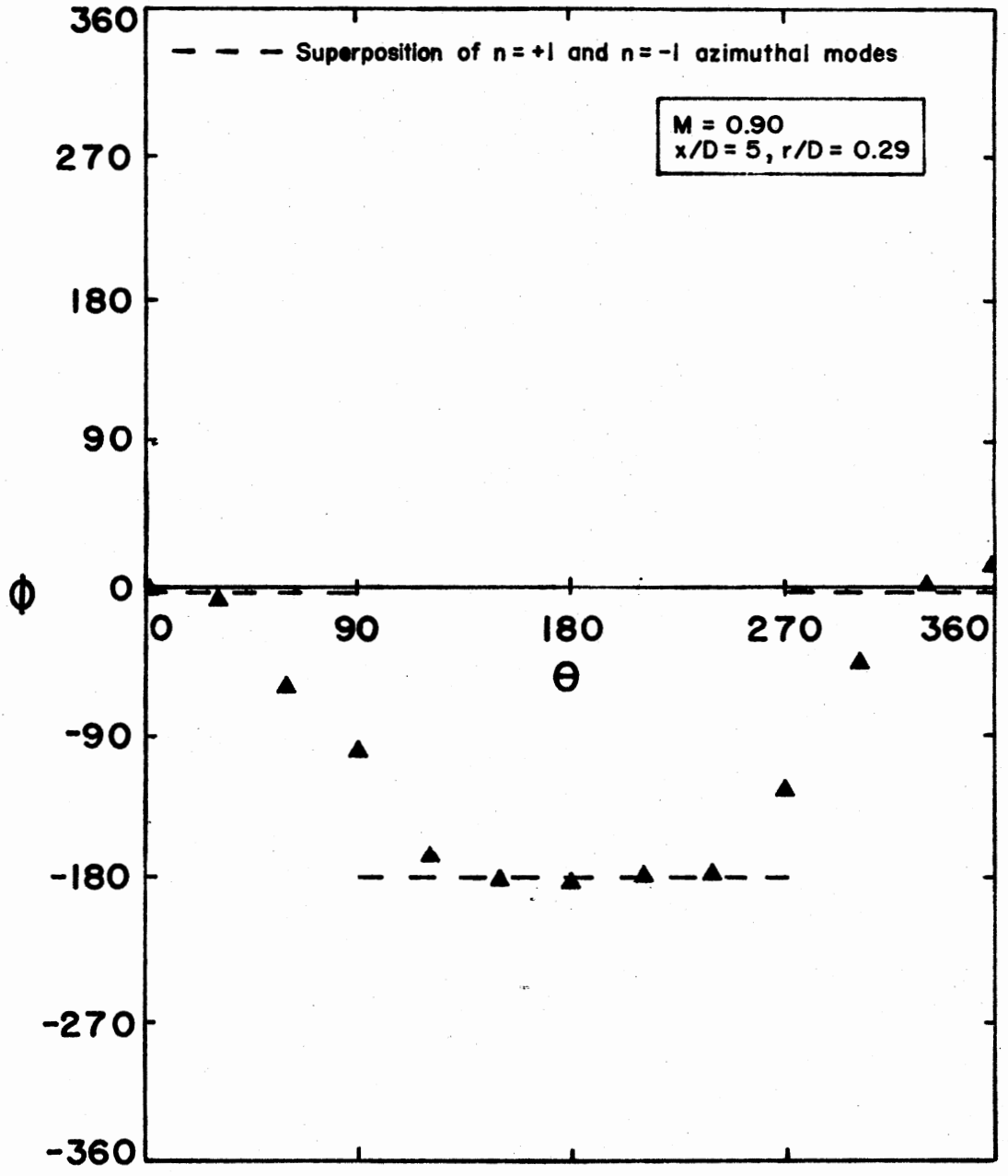

Figure 22. Averaged Distribution of Azimuthal Phase (Flowfield), St = 0.44 Component, Mach Number 0.90

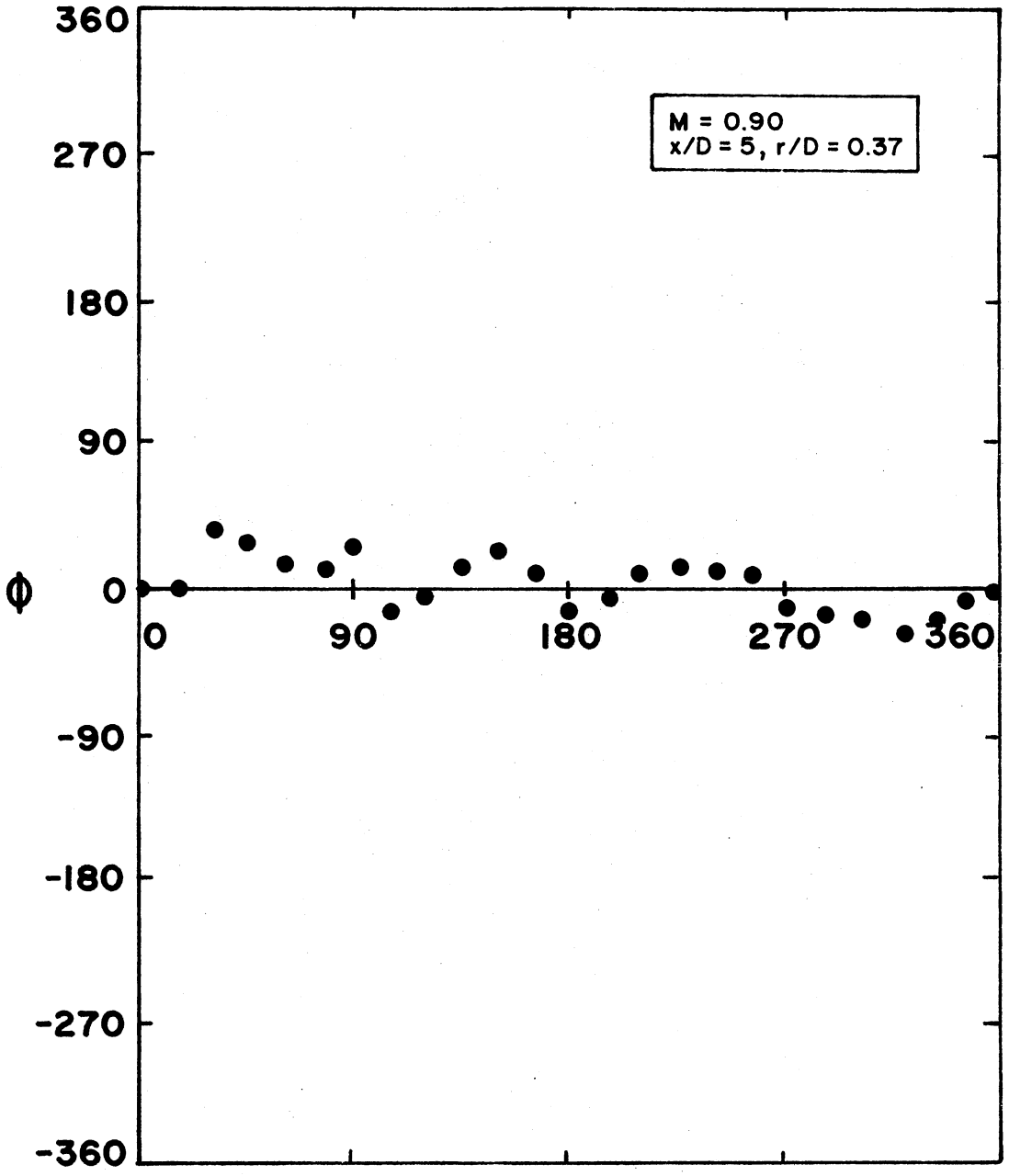

Figure 23. Distribution of Azimuthal Phase (Flowfield), St = 0.22 Component, Mach Number 0.90

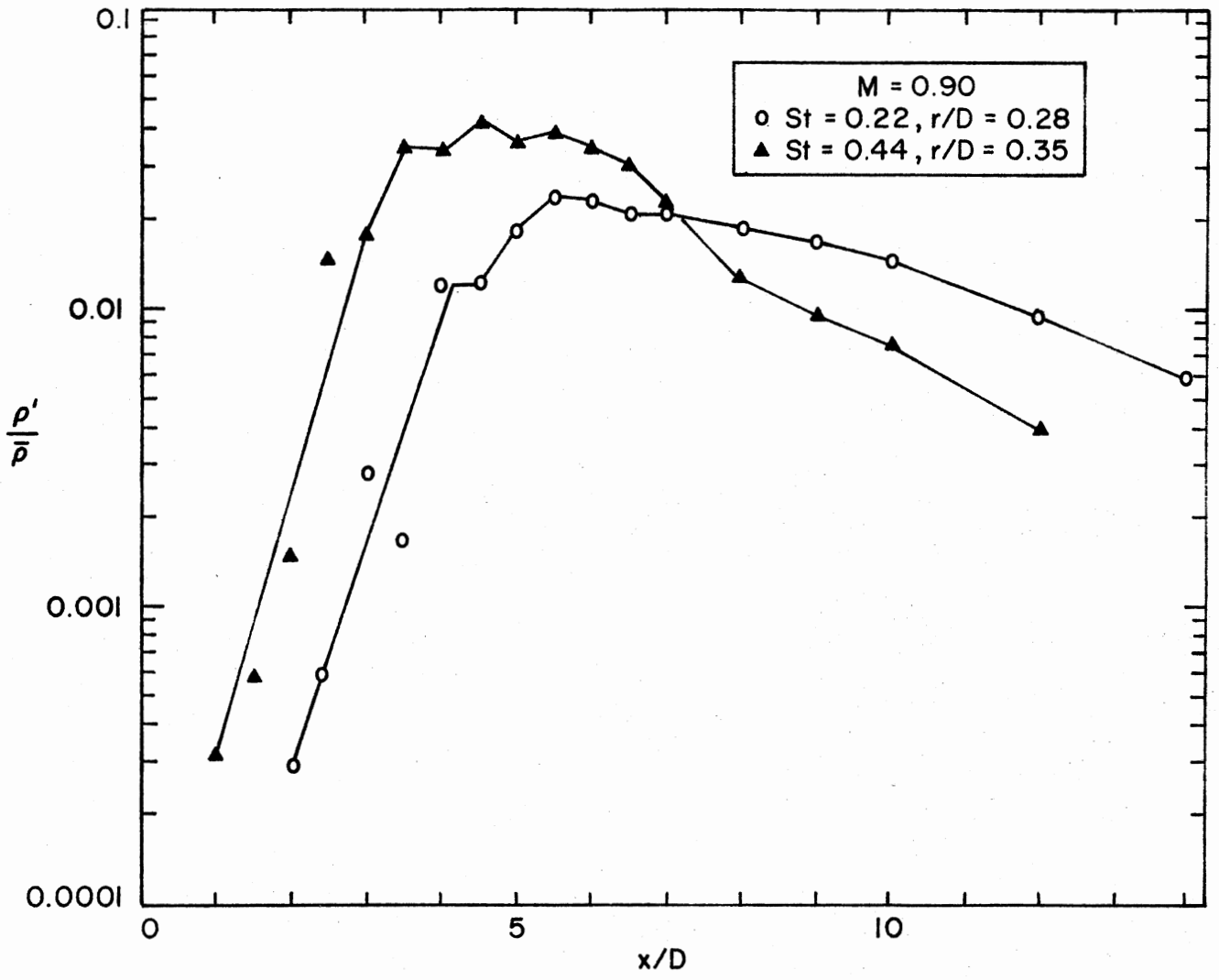

Figure 24. Axial Distribution of $\rho'/\bar{\rho}$, St = 0.22 and 0.44 Components, Mach Number 0.90

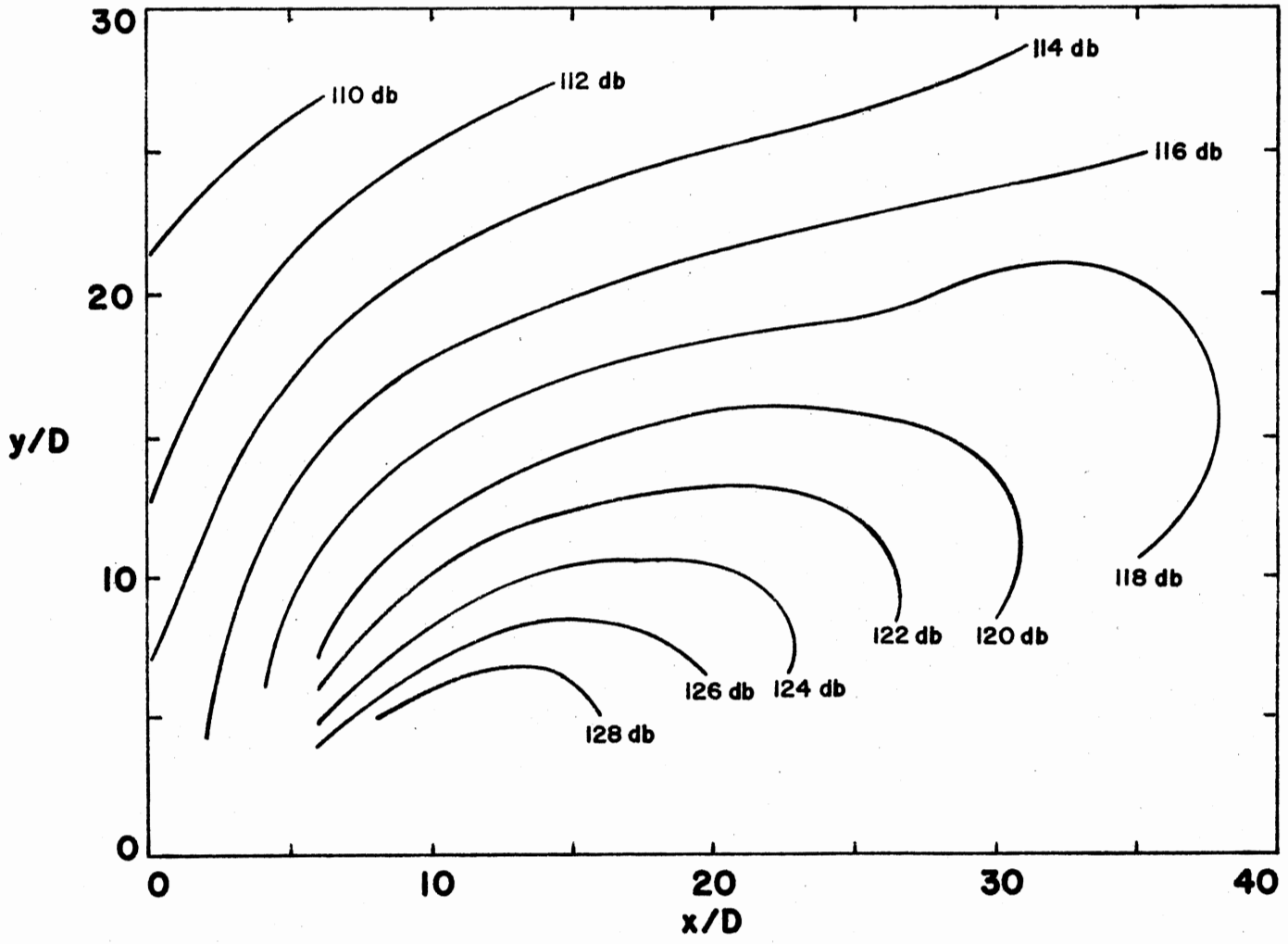

Figure 25. Sound Pressure Level Contours, Mach Number 0.90 (Low Reynolds Number)

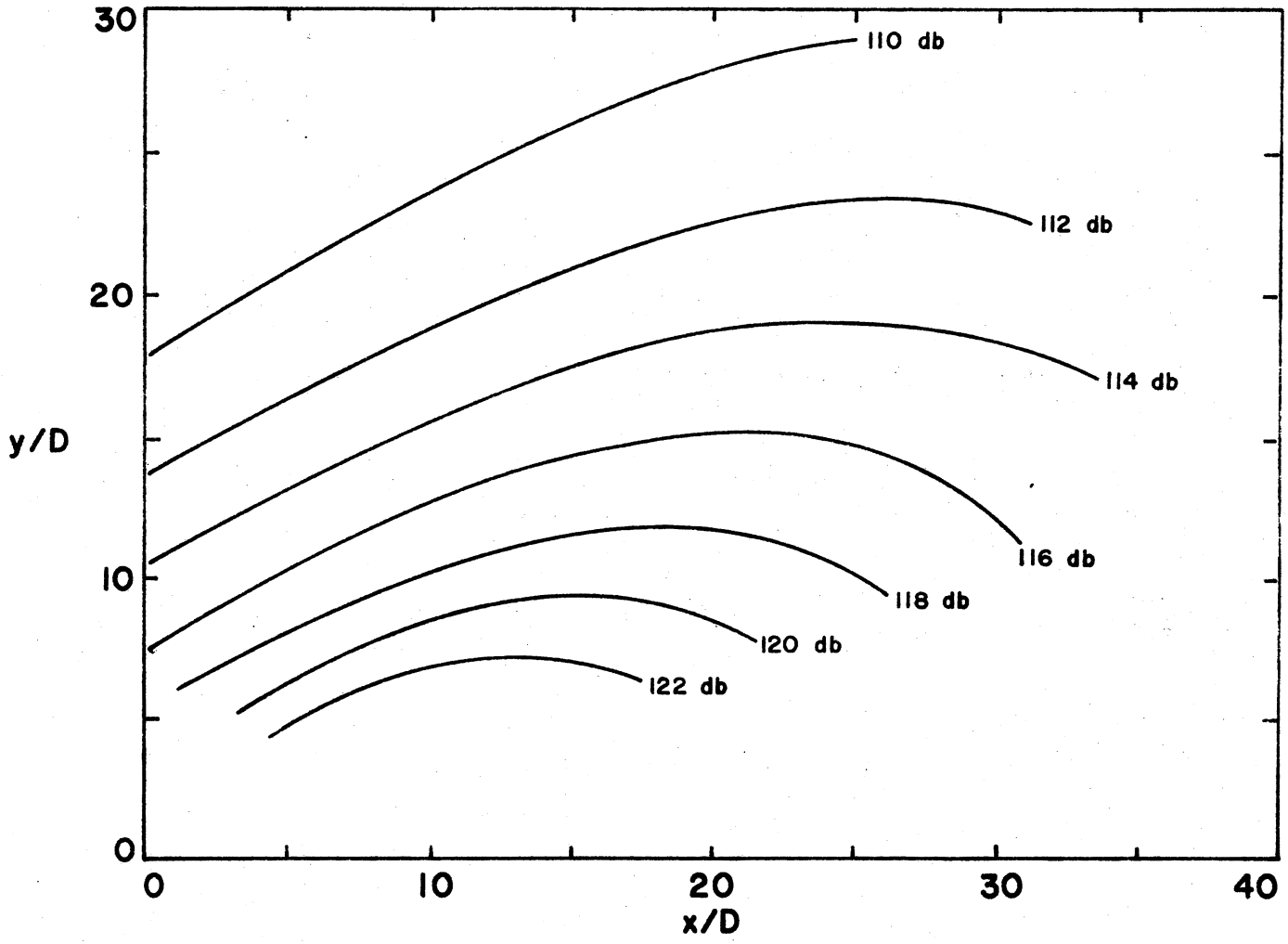

Figure 26. Sound Pressure Level Contours, Mach Number 0.90 (High Reynolds Number)

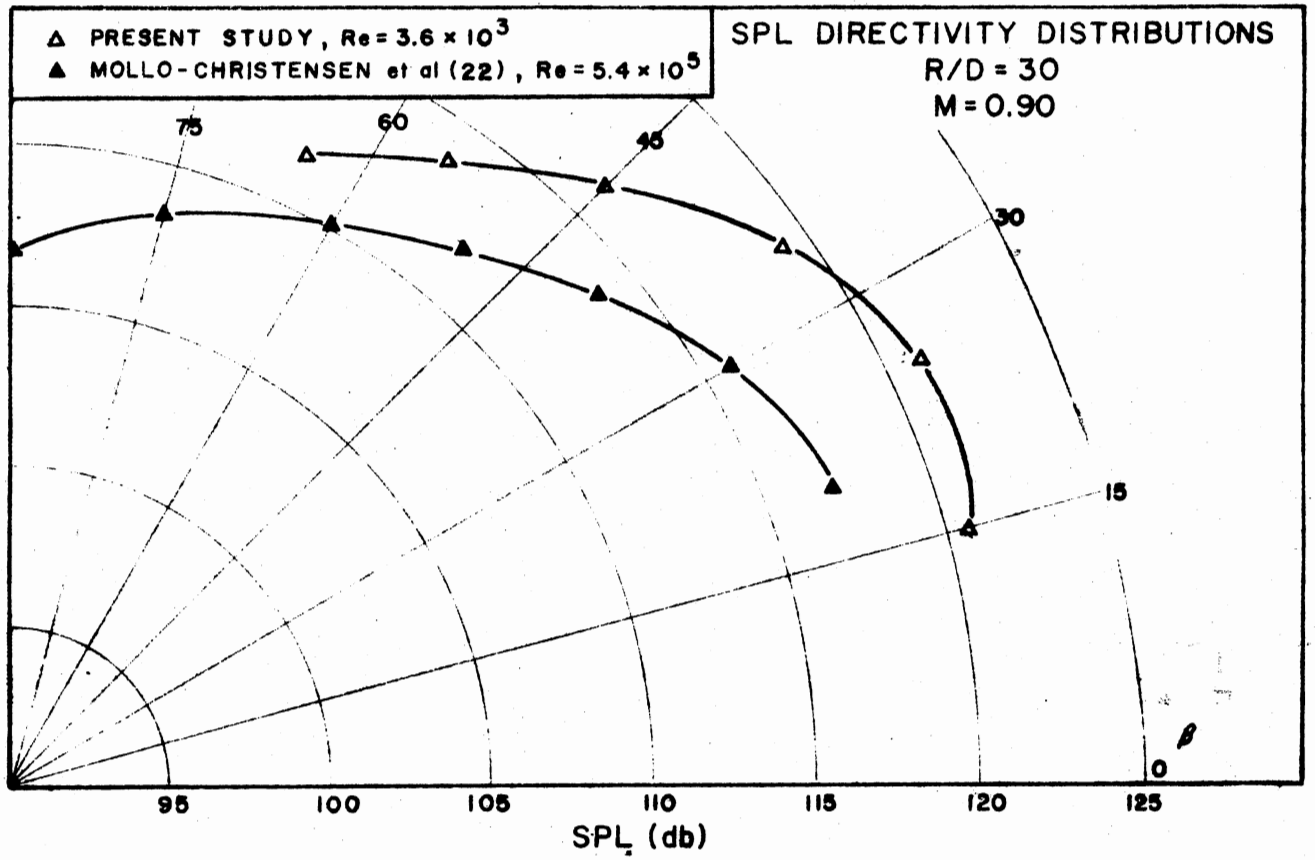

Figure 27. Sound Pressure Level Directivity Distribution, Mach Number 0.90

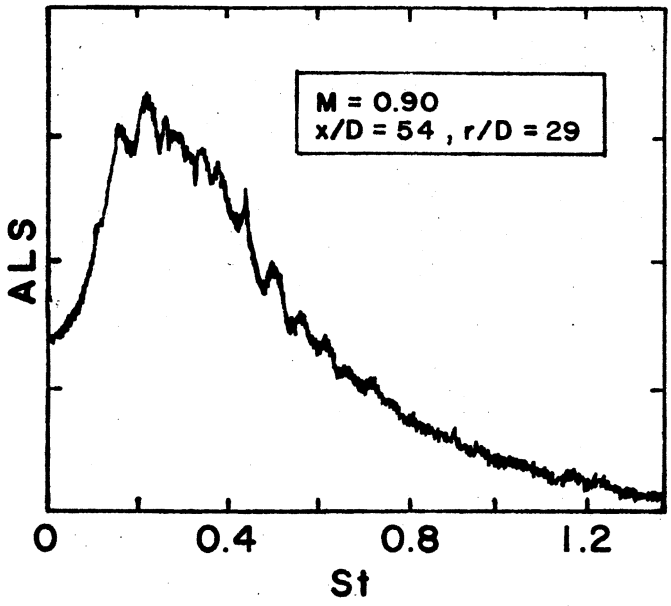

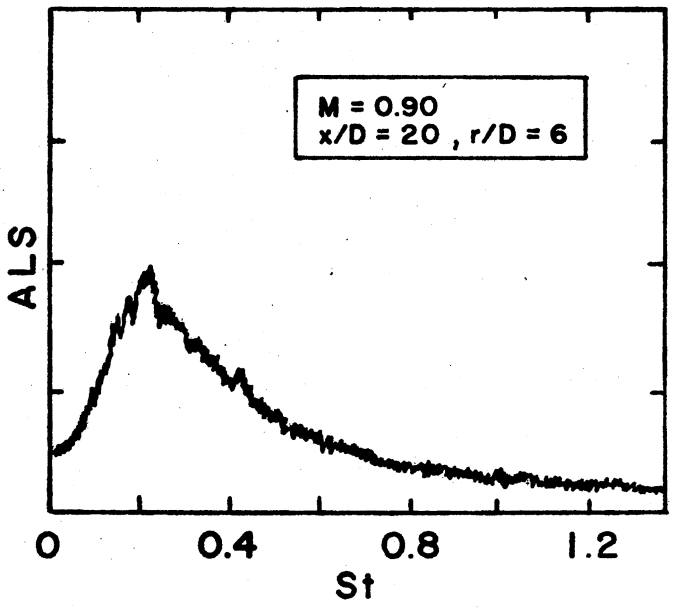

Figure 28. Microphone Spectra, Mach Number 0.90

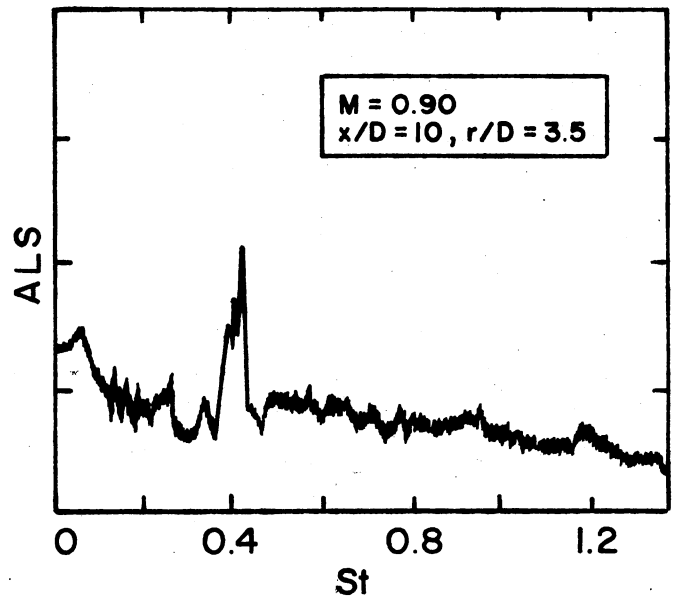

Figure 29. Near Field Microphone Spectrum, Mach Number 0.90

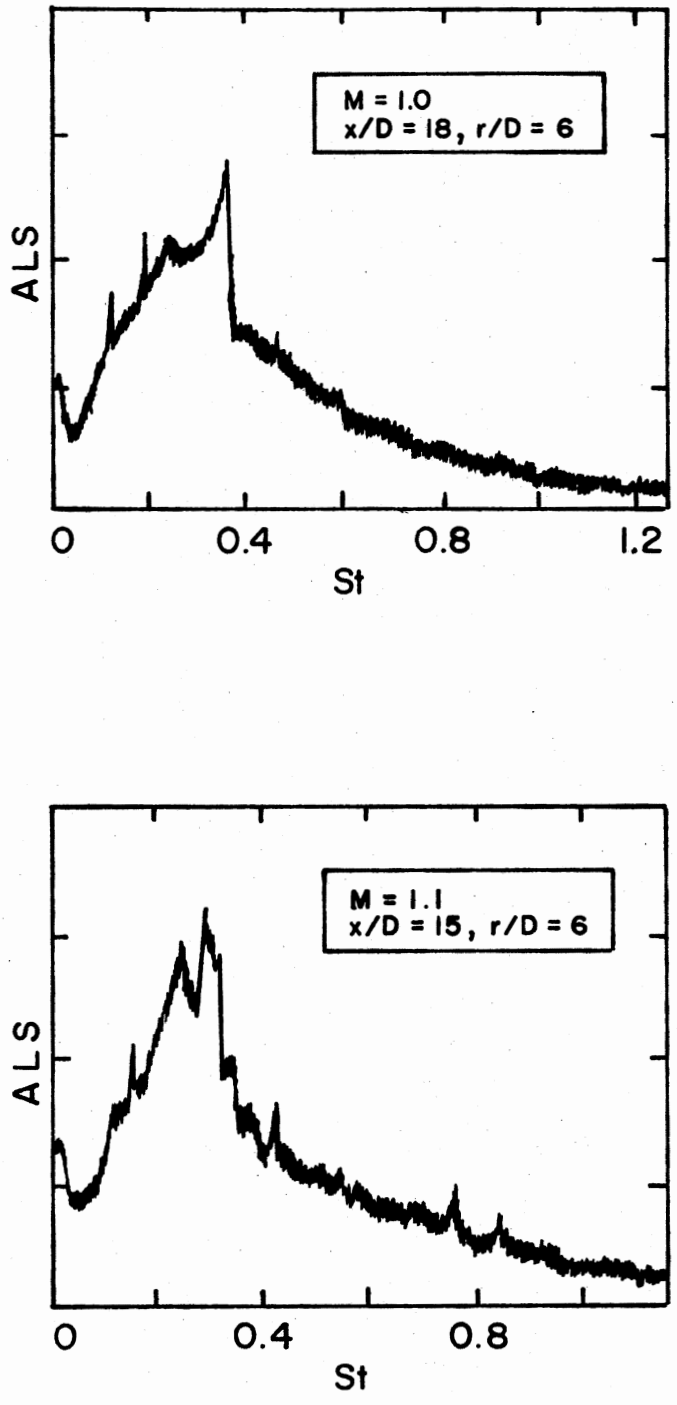

Figure 30. Microphone Spectra in Maximum SPL Lobe, Mach Numbers 1.0 and 1.1

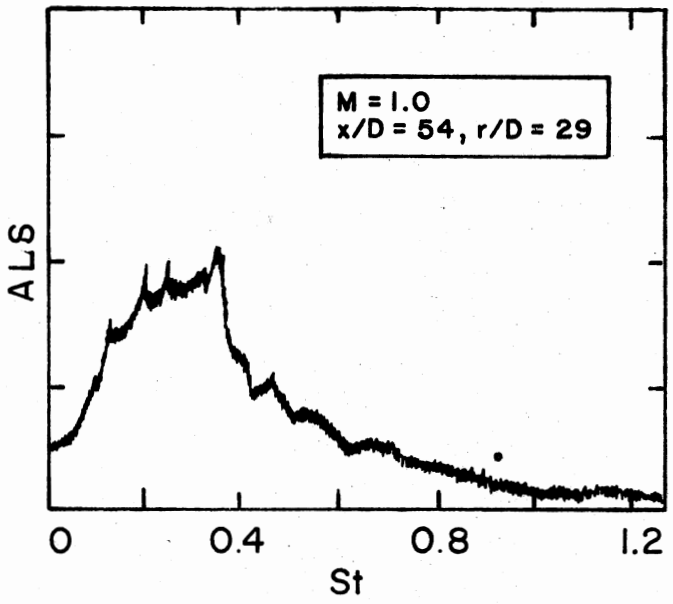

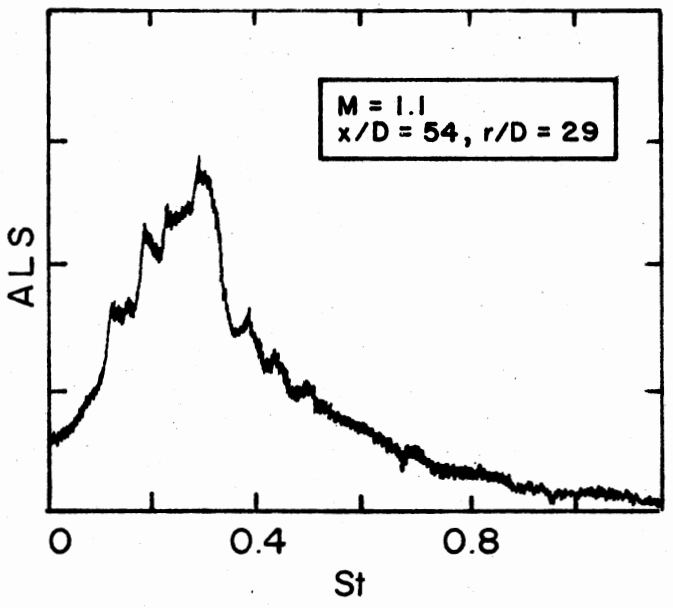

Figure 31. Far Field Microphone Spectra, Mach Numbers 1.0 and 1.1

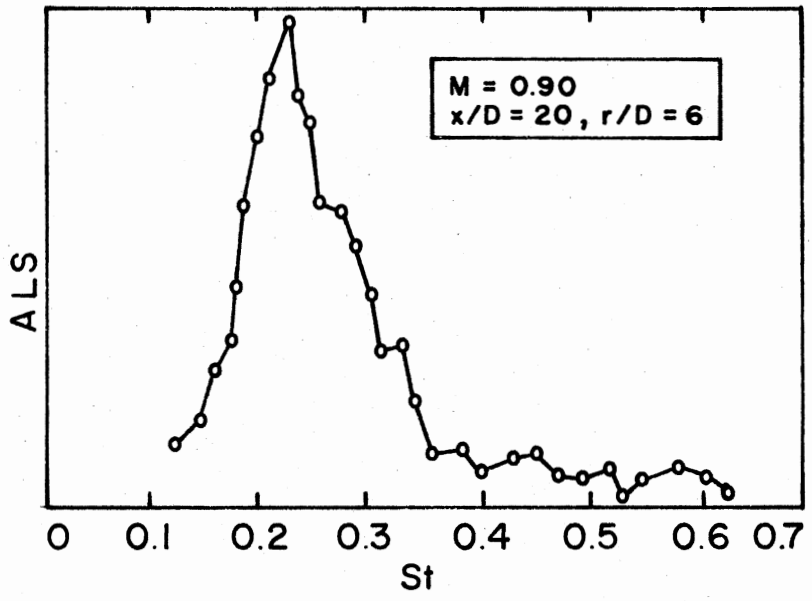

Figure 32. Acoustic Field Response to Excitation, Mach Number 0.90

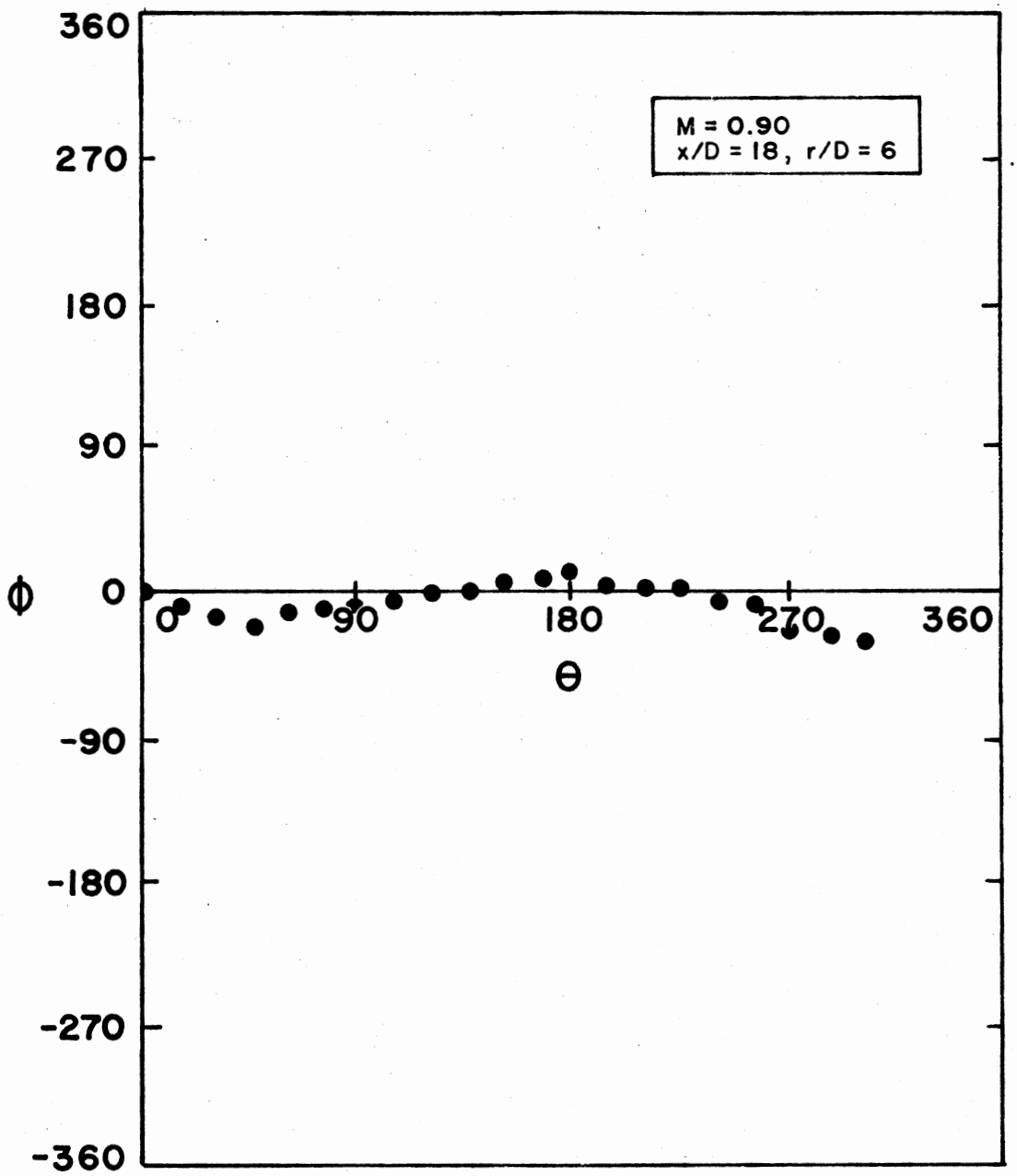

Figure 33. Distribution of Azimuthal Phase (Acoustic Field), St = 0.22 Component, Mach Number 0.90.

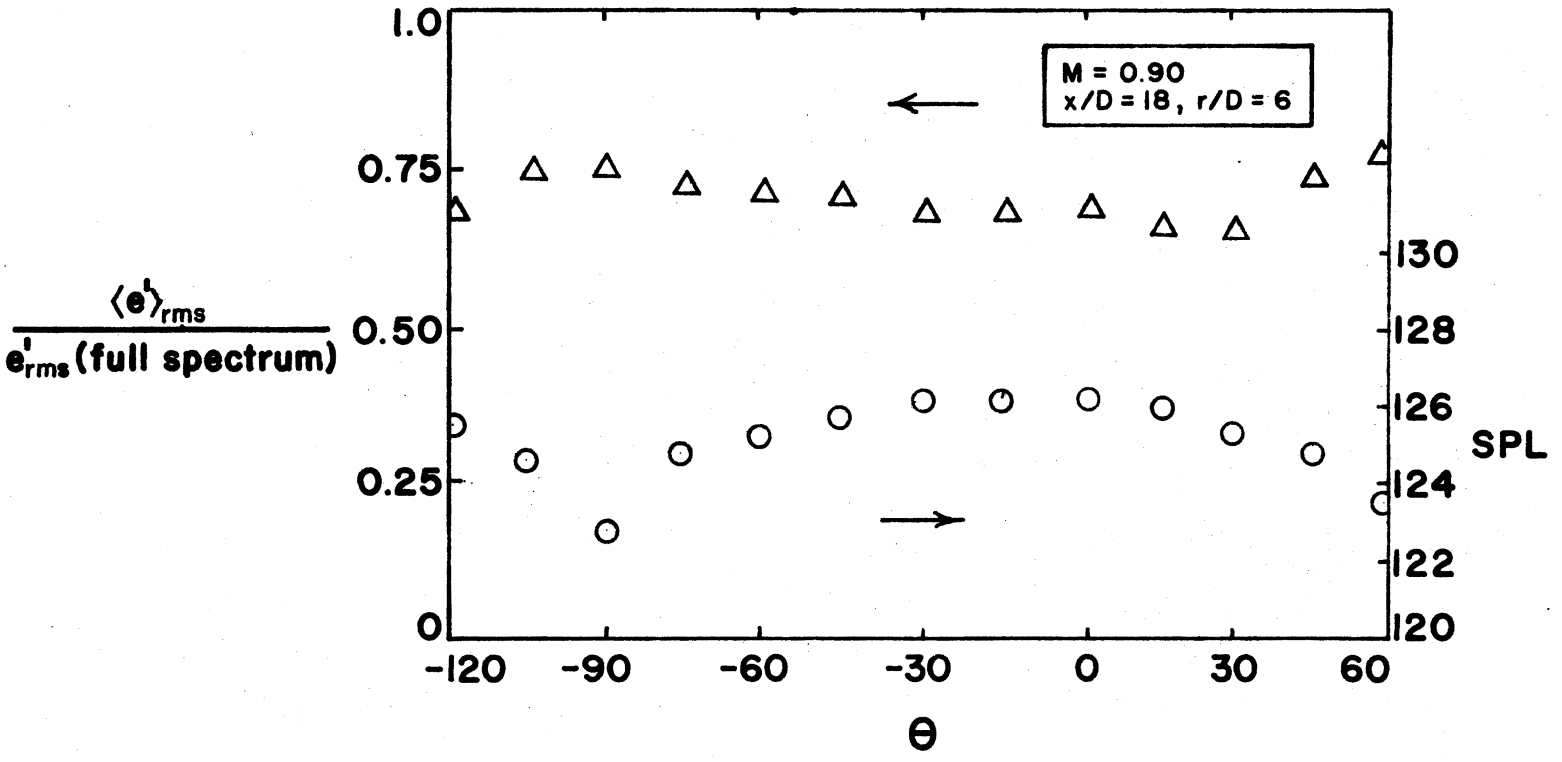

Figure 34. Azimuthal Distribution of SPL and Acoustic Coherence, Mach Number 0.90

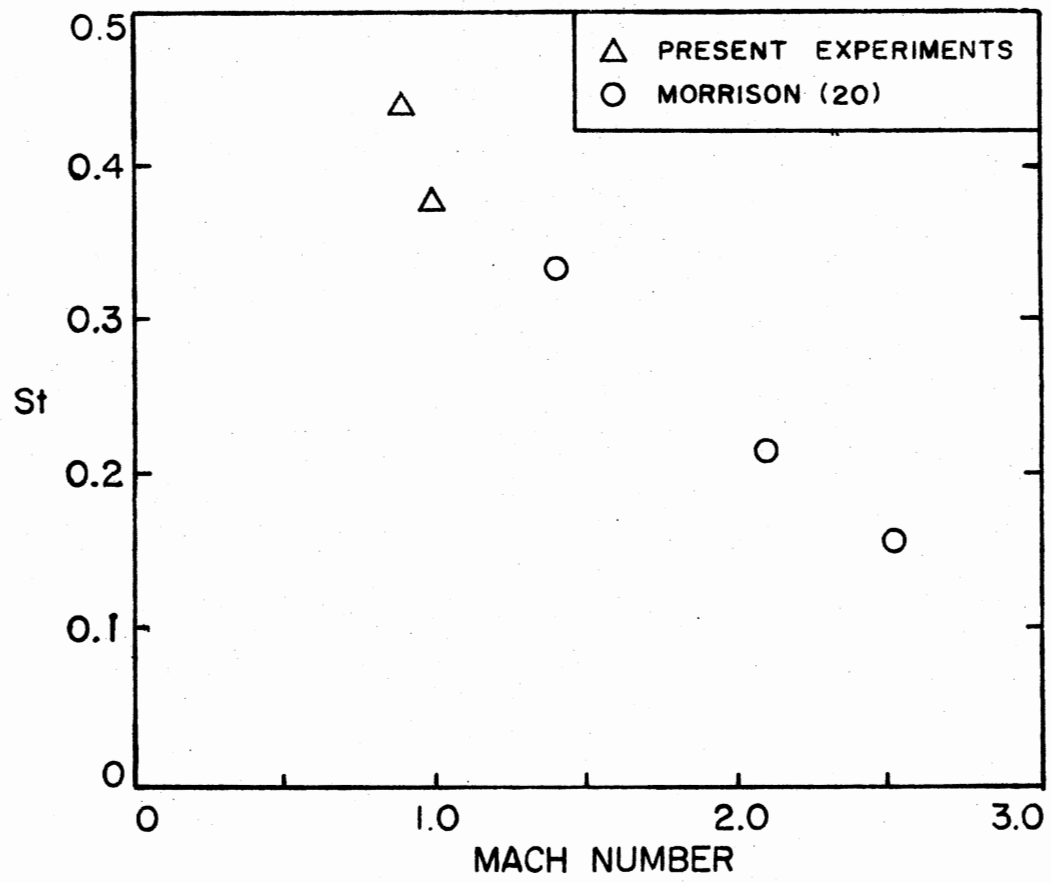

Figure 35. Strouhal Number Variation With Mach Number

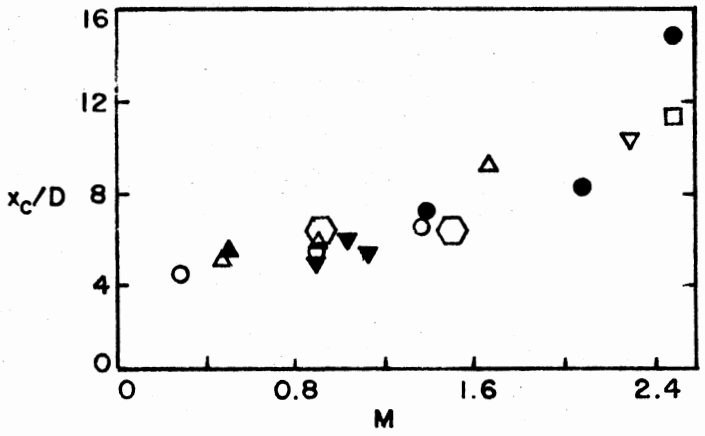

Sources:

- ▼ Present study
- O Lau et al. (29)
- ▲ Knott and Mossey (30)
- △ Morris (31)
- □ Potter and Jones } see (32)
- ▽ Eggers } see (32)
- ⬡ Warren
- ● Morrison (20)

Figure 36. Length of Potential Core as a Function of Mach Number

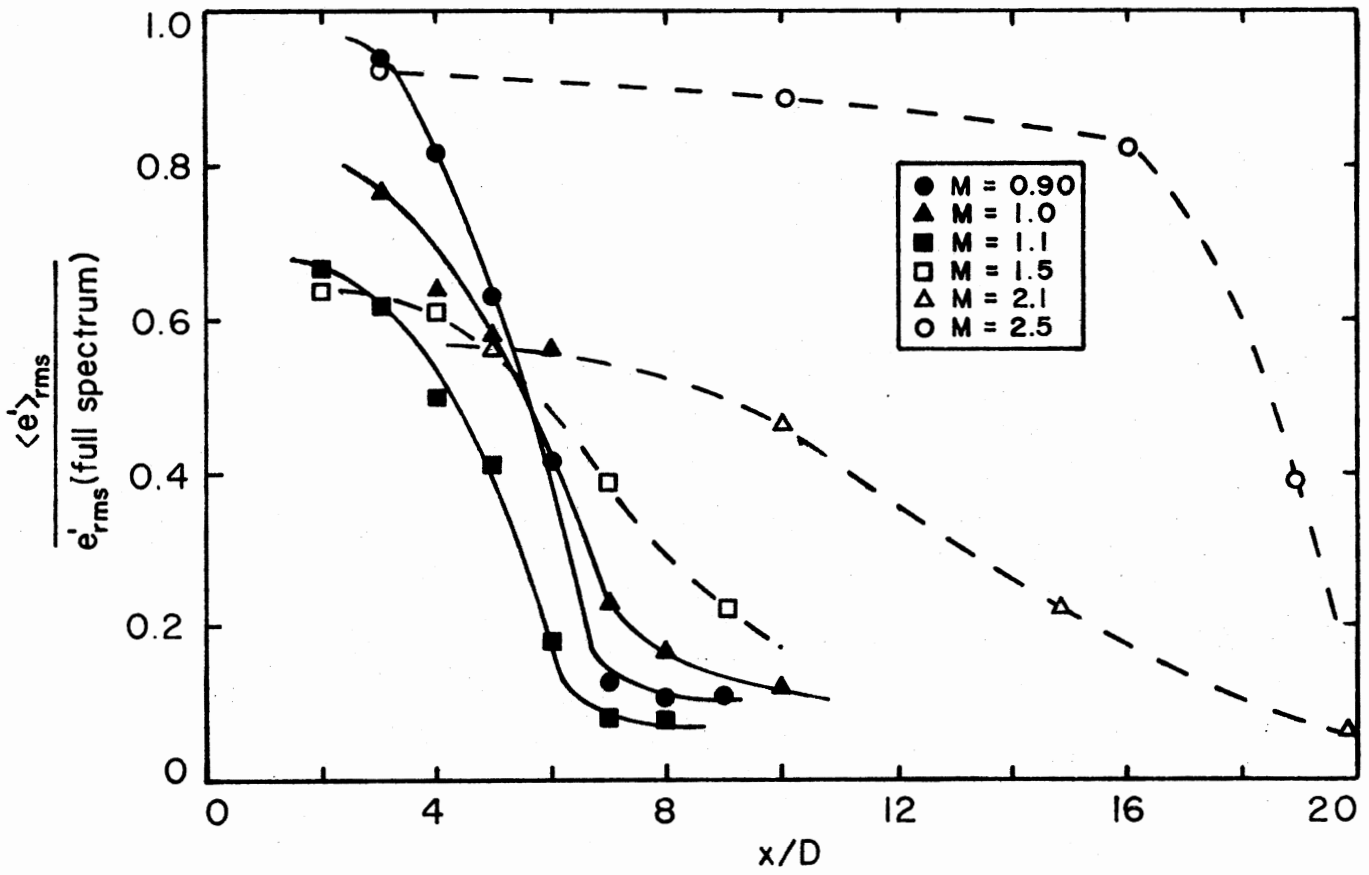

Figure 37. Axial Distribution of the Fraction Coherent Structure in the Flow

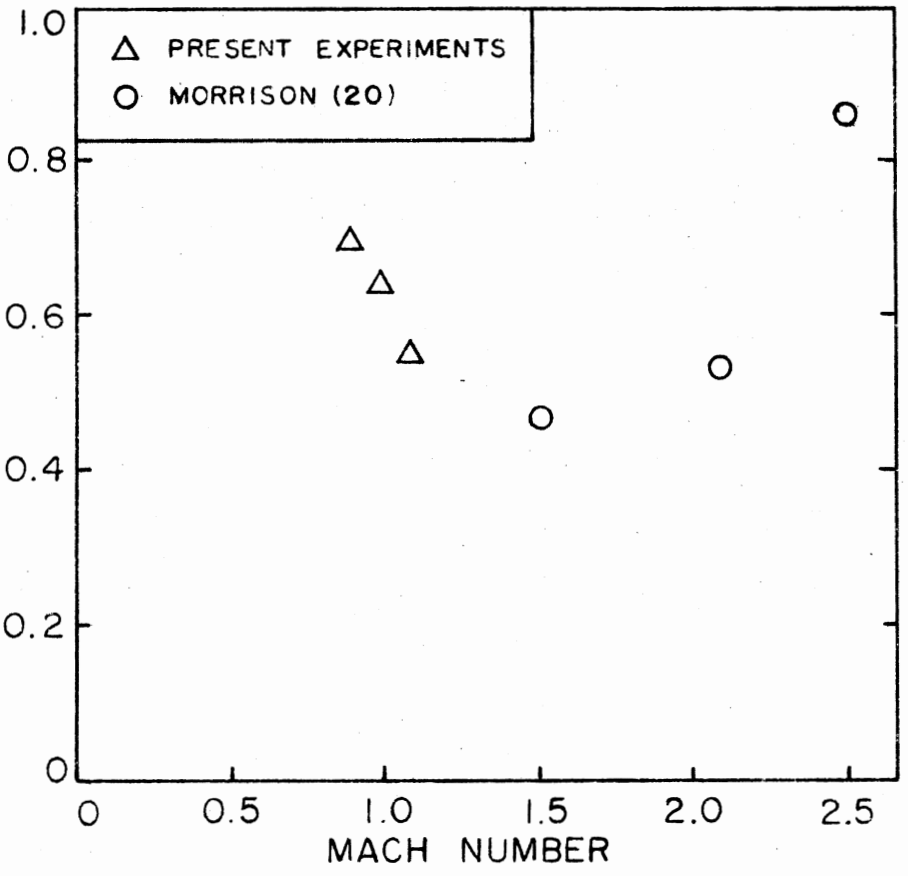

Figure 38. Average Fraction Coherent Structure as a Function of Mach Number

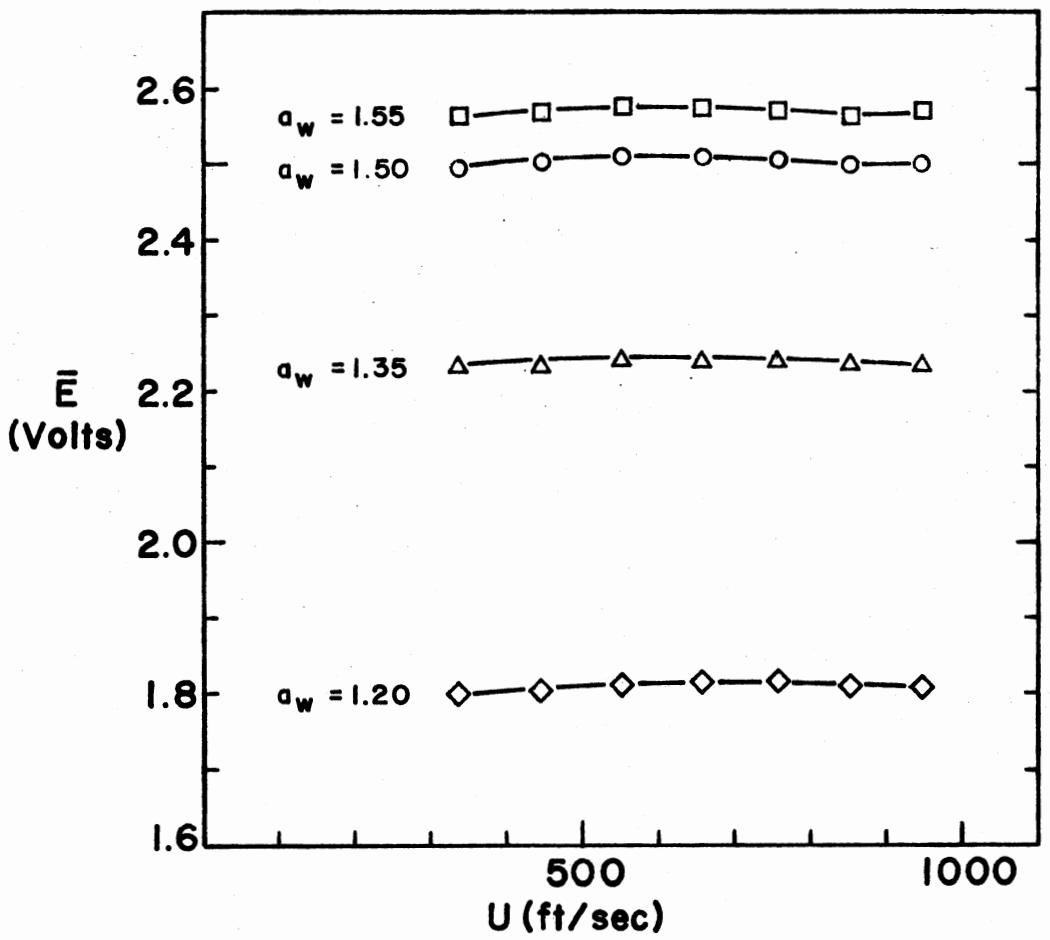

Figure 39. Hot-Wire Calibration, u versus $\bar{E}$

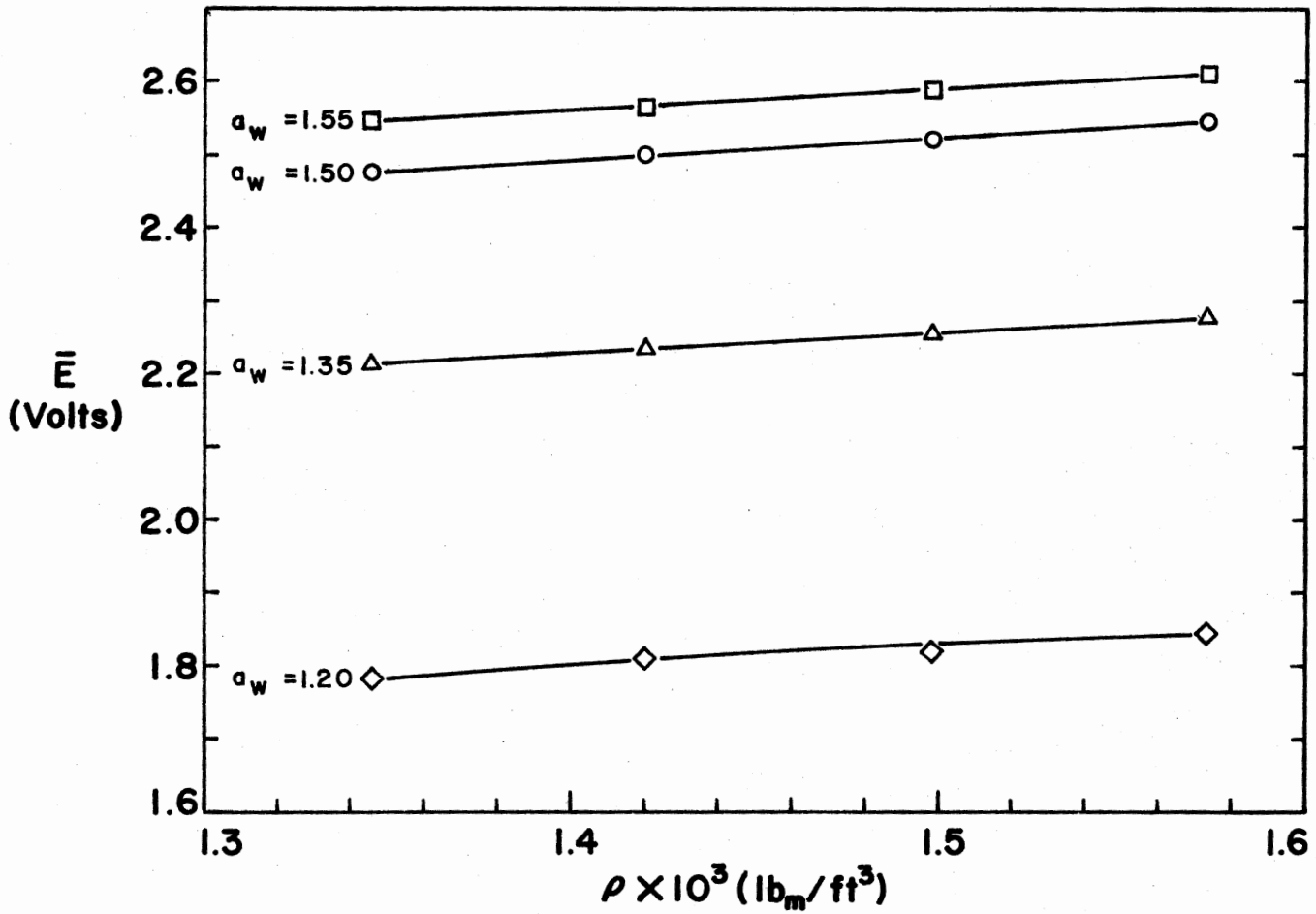

Figure 40. Hot-Wire Calibration, ρ versus $\bar{E}$

VITA[2]

James Lynn Stromberg

Candidate for the Degree of

Master of Science

Thesis: FLOWFIELD AND ACOUSTIC MEASUREMENTS OF LOW REYNOLDS NUMBER JETS IN THE TRANSONIC RANGE

Major Field: Mechanical Engineering

Biographical:

Personal Data: Born in Stillwater, Oklahoma, December 10, 1947.

Education: Graduated from Tucson High School, Tucson, Arizona, in January, 1966; received the Bachelor of Science in Mechanical Engineering degree from Oklahoma State University in December, 1976; completed requirements for the Master of Science degree at Oklahoma State University in July, 1978.